Coexisting Terahertz and RF Finite Wireless Networks: Coverage and Rate Analysis

Nour Kouzayha, *Member, IEEE*, Mustafa A. Kishk, *Member, IEEE*, Hadi Sarieddeen, *Member, IEEE*, Mohamed-Slim Alouini, *Fellow, IEEE*, and Tareq Y. Al-Naffouri, *Senior Member, IEEE*

***Abstract*— Wireless communications over Terahertz (THz)-band frequencies are vital enablers of ultra-high rate applications and services in sixth-generation (6G) networks. However, THz communications suffer from poor coverage because of inherent THz features such as high penetration losses, significant molecular absorption, and severe path loss. To surmount these critical challenges and fully exploit the THz band, we explore a coexisting radio frequency (RF) and THz finite indoor network in which THz small cells are deployed to provide high data rates, and RF macrocells are deployed to satisfy coverage requirements. Using stochastic geometry tools, we assess the performance of coexisting RF and THz networks and derive tractable analytical expressions for the coverage probability and average achievable rate. The analytical results are validated with Monte-Carlo simulations. Several insights are devised for accurate tuning and optimization of THz system parameters, including the THz bias, and the fraction of THz access points (APs) to deploy. The obtained results recognize a clear coverage/rate trade-off where a high fraction of THz AP improves the rate significantly but may degrade the coverage performance. Furthermore, the location of a user in the finite area highly affects the fraction of THz APs that optimizes its quality of service.**

***Index Terms*— Terahertz (THz) communications, radio frequency (RF) communications, finite indoor network, coverage probability, average achievable rate, stochastic geometry.**

I. Introduction

FOLLOWING the successful implementation of millimeter-wave (mmWave) technology in the fifth generation (5G) of wireless communications [1], terahertz (THz) communications are being envisioned as critical enablers for alleviating spectrum scarcity and breaking the capacity limitation in the sixth generation (6G) of wireless networks [2], [3], [4], [5]. Specifically, the ultra-wide THz band that ranges from 0.1 THz to 10 THz promises to support applications with high quality of service characteristics and terabits per seconds data rates. Furthermore, THz networks can realize secure communications and massive connectivity with plenty of available spectrum resources as more than 10 billion devices are expected to be connected in the coming years [6]. The THz band also provides a remarkable potential for enabling accurate sensing and localization [2], [7].

Despite the vision and promise of the THz technology, the unique properties of THz wave propagation impose several challenges that hinder the deployment of THz networks [8], [9]. For instance, compared to lower frequencies, atmospheric effects can significantly degrade THz propagation and result in high spreading and molecular absorption losses [10]. Such losses decrease the THz transmission distance and cell size, which requires accurate planning for THz network deployments [11]. Moreover, high reflection and scattering losses are encountered at high frequencies, which causes the attenuation of non-line-of-sight (NLoS) paths as the power of the received signal becomes very low when reflected or scattered [10], [12]. Furthermore, due to the short wavelengths, THz communications are highly vulnerable to the existence of small blockages such as the user itself or moving humans in the environment [13]. These blockages cause significant attenuation to THz propagation because of the high penetration loss, further decreasing the THz transmission range. To cope with the limited range of THz networks and due to the use of higher frequencies, ultra-dense deployments and highly directional antennas are envisioned in THz networks. However, such deployments significantly increase the interference, limiting network density and pose challenges with respect to beam alignment and tracking [14]. The distinctive features and challenges of THz communications motivate the design of new solutions to address all these challenges and efficiently deploy THz networks [15], [16].

Because of their limited bandwidth, sub-6 GHz technologies cannot cope with very high data-rate demands. Integrating small cells that operate in the THz band is fundamental to satisfying the increasing need for ultra-high data rates; keeping some sub-6 GHz cells can surpass the limited coverage of THz communications. Furthermore, THz systems are expected to provide attractive wireless backhaul solutions to sub-6 GHz networks, when deploying fiber is costly

Manuscript received 7 October 2021; revised 14 July 2022 and 28 November 2022; accepted 4 December 2022. Date of publication 22 December 2022; date of current version 12 July 2023. This work was supported by the King Abdullah University of Science and Technology (KAUST) Office of Sponsored Research (OSR) under Award ORA-CRG2021-4695. The associate editor coordinating the review of this article and approving it for publication was C. Masouros. *(Corresponding author: Nour Kouzayha.)*

Nour Kouzayha, Mohamed-Slim Alouini, and Tareq Y. Al-Naffouri are with the Division of Computer, Electrical and Mathematical Sciences and Engineering, King Abdullah University of Science and Technology, Thuwal 23955, Saudi Arabia (e-mail: nour.kouzayha@kaust.edu.sa; slim.alouini@kaust.edu.sa; tareq.alnaffouri@kaust.edu.sa).

Mustafa A. Kishk is with the Department of Electronic Engineering, National University of Ireland, Maynooth, W23 F2H6 Ireland (e-mail: mustafa.kishk@mu.ie).

Hadi Sarieddeen is with the Research Laboratory of Electronics, Massachusetts Institute of Technology, Cambridge, MA 02139 USA (e-mail: hadisari@mit.edu).

Color versions of one or more figures in this article are available at https://doi.org/10.1109/TWC.2022.3229745.

Digital Object Identifier 10.1109/TWC.2022.3229745

or infeasible [17]. This work presents a comprehensive analytical framework using stochastic geometry to characterize the coverage probability and average achievable rate in a coexisting RF and THz finite indoor network. THz small cells are deployed to provide high data rates while RF macrocells are deployed to satisfy coverage requirements.

A. Related Work

Stochastic geometry is used extensively for studying various aspects of wireless networks, characterizing their functionality, and understanding their operation [18]. In THz systems, although narrow THz beam widths result in less interference, excessive inter-cell interference is experienced because of the dense deployment of THz base stations needed to compensate for the high path and molecular absorption losses. This further motivates the use of stochastic geometry thanks to its capability of introducing a mathematically compliant formulation for the interference in the network analysis, which is incredibly challenging with other techniques.

Using tools from stochastic geometry, several works are developed in the literature to study the performance of networks operating in the THz frequency band. To date, the majority of existing research works focus on studying the performance of THz-only networks [19]. Furthermore, most of these works study the mean interference power and signal to interference and noise ratio (SINR) and their moments, rather than characterizing the coverage probability and average rate [20], [21], [22], [23]. In [20], [21], and [22], the performance of THz networks is studied using stochastic geometry while taking into consideration both the effect of indoor blockages and directional antennas. However, the reliability of these models is limited as they rely mainly on approximations. For instance, the authors in [20] approximate the mean and variance of the interference and the SINR using Taylor expansion. In [21] and [22], the mean interference is used instead of the instantaneous interference in deriving the coverage probability of the THz network. The work in [24] uses the central limit theorem and the normal distribution to approximate the interference and obtain the coverage probability in a user-centric THz network where several base stations (BSs) cooperate to serve each user.

Two-dimensional (2D) architectures are usually used in modeling sub-6 GHz networks to simplify the analysis and derive tractable performance metrics. While it may be acceptable to neglect the effect of vertical heights in sub-6 GHz networks because of the large transmission distance, such assumption is inaccurate for dense THz networks with limited transmission ranges [25]. Recently, few papers in the literature have determined the coverage probability of a THz network in a three-dimensional (3D) indoor environment [26], [27], [28], [29] in which THz transmitters are mounted on the ceiling with fixed height to serve users. These works show the impact of different blockage types, including walls and moving humans, on the reliability performance of THz networks [27], [28]. While small scale fading is ignored in [28] and [29], the authors in [27] develop a statistical framework for the indoor THz channel. This framework accounts for the line-of-sight (LoS) and NLoS THz communications in indoor environments and approximates the fading distribution from the multi-ray THz channel model.

Despite the coverage limitations of THz communications, modeling and analyzing hybrid RF/THz networks to satisfy coverage and high rate requirements is not yet thoroughly investigated [30]. Most of the works in literature are focused on assessing the performance of THz-only networks while characterizing THz propagation accurately. While it is true that RF and THz communications have orthogonal spectrum and do not interfere with each other, considering them as two standalone systems is inaccurate and any pre-deployment planning should optimize both systems simultaneously to guarantee best service to users. The work in [31] is one of the few exceptions that considers a coexisting sub-6 GHz and dense THz wireless network. However, this work only focuses on a 2D environment and does not account for the impact of beam steering errors, which can significantly affect the THz transmission. In addition, the infinite Poisson point process (PPP) is used to model the THz network in [31], which does not fit realistic indoor use cases of THz deployment. The work in [32] considers a THz-only network while accounting for the finite nature of the THz network and evaluates the performance of both central users and edge users. Another heterogeneous network consisting of macro BSs that operate at sub-6 GHz, unmanned aerial vehicles (UAVs) that operate at mmWave frequencies, and small BSs using both mmWave and THz communications is proposed in [33]. However, this work captures the impact of blockages on mmWave communications only and ignores it for THz communications. In [34], the authors study and compare different user association strategies schemes and multi-connectivity strategies for hybrid THz/mmWave networks. To the best of the authors' knowledge, none of the previous research works presented a comprehensive analytical framework to characterize coverage probability and rate in a coexisting RF and THz finite indoor network. As a result, this work aims to address the details of this problem using stochastic geometry and to devise useful recommendations for THz deployment.

B. Contributions

This paper considers a hybrid RF/THz finite network, where THz and RF APs coexist to provide coverage and throughput for users in a realistic indoor environment. The THz APs use directional antennas to cope with high loss levels and limited coverage of THz communications and are affected by existing blockages in the environment and beam-steering errors of directional antennas. While the blockage model by itself is not novel and has been used previously in [28], its application in a coexisting RF/THz network is new. Using tools from stochastic geometry, our goal is to assess the performance of the coexisting RF and THz network and to highlight the impact of different system parameters. To this extent, the main contributions of this paper can be described as follows:

- We consider a realistic indoor environment where a finite number of RF and THz APs coexist to provide users

with coverage and rate. We model the APs network as a binomial point process (BPP), fitting more realistic finite indoor applications than the infinite PPP used in most literature works. Furthermore, the BPP captures the performance variability for a given user location and allows for better analysis of the RF/THz coexisting system. The developed model accounts for the molecular absorption loss, which significantly affects the THz propagation. Furthermore, an accurate analytical model is used to account for self-blockage, human blockages and walls blockages in the environment, in addition to the directional antennas at both the THz APs and users and the resulting beam-steering errors.

- We devise a tractable analytical framework, using tools from stochastic geometry, to characterize the coverage probability and average achievable rate of the coexisting RF and THz network. Specifically, we derive the association probabilities with an RF AP and a THz AP and the conditional coverage probabilities and average rates. Finally, we use the law of total probability to determine the considered metrics. Unlike earlier works, the proposed analytical framework provides exact expressions for the coverage probability and average rate rather than relying on approximations. The analytical results are validated using Monte-Carlo simulations and can be traced, validated, reproduced, and utilized by interested researchers and system engineers.
- Based on the developed framework, we study how different system parameters affect the network performance. Such parameters include the fraction of THz APs and the total number of APs, the THz bias term, the location of the user in the finite area, the density of blockages and the beam-steering errors. The obtained results capture the coverage/rate trade-off imposed by densifying the network with THz APs and devise useful design guidelines for the deployment and optimization of THz networks.

C. Organization and Notations

Throughout the paper, the subscripts $\{\cdot\}_{\mathrm{A}}$ and $\{\cdot\}_{\mathrm{U}}$ refer to AP and user, respectively. The subscripts $\{\cdot\}_{\mathrm{T}}$ and $\{\cdot\}_{\mathrm{R}}$ indicate THz and RF communications. The subscripts $\{\cdot\}_{\mathrm{L}}$, $\{\cdot\}_{\mathrm{N}}$ differentiate between THz LoS and THz NLoS, respectively. The symbols $\mathbb{P}\{\cdot\}$ and $||\cdot||$ refer to probability and euclidean norm, while $\mathbb{E}[\cdot]$, $\mathcal{L}_x(\cdot)$, and $\mathcal{W}[\cdot]$ denote the expectation, the Laplace transform of a random variable x, and the Lambert W-function defined as the inverse function of $f(w) = we^w$, respectively. The rest of notations are presented in Table I.

The remainder of the paper is organized as follows. We describe the RF and THz coexisting system model in Section II. Section III derives the association probabilities and serving distance distributions. These distributions are in turn used in Section IV to derive the coverage probability and the average achievable rate. Numerical results are discussed in Section V and validated using Monte-Carlo simulations. Finally, we conclude the paper in Section VI.

TABLE I
NOTATIONS SUMMARY

Notation	Description
r_d	Radius of the disk in which the APs are distributed
h_{A}	Height of the APs with reference to the ground level
N_{A}	Number of APs
v_0, h_{U}, ω_{S}	Distance from the UE to origin, height of UE from the ground level, self-blocking angle
Φ_{A}, Φ_{R}, Φ_{T}, Φ_{L}, Φ_{N}	Set of APs, RF APs, THz APs, LoS THz APs, or NLoS THz APs, respectively
δ_{T}	Fraction of THz APs
$\kappa_{\mathrm{L}}(\cdot)$, $\kappa_{\mathrm{N}}(\cdot)$	Probability of the THz AP having a LoS or a NLoS connection with the UE, respectively
P_{R}, P_{T}	Transmit power of RF and THz APs, respectively
W_{R}, W_{T}	RF and THz bandwidths, respectively
f_{R}, f_{T}	RF and THz carrier frequencies, respectively
$k_a(f_{\mathrm{T}})$	THz molecular absorption coefficient
σ^2_{R}, σ^2_{T}	Noise power of RF and THz communications, respectively
α_{R}, α_{L}, α_{N}	Path-loss exponent parameter for RF, LoS THz, or NLoS THz, respectively
m_{L}, m_{N}	Nakagami-m fading parameter for LoS THz, and NLoS THz, respectively
$G^{\max}_{\mathrm{T}}$, $G^{\min}_{\mathrm{T}}$, φ_{T}	Antenna parameters for THz AP
$G^{\max}_{\mathrm{U}}$, $G^{\min}_{\mathrm{U}}$, φ_{U}	Antenna parameters for UE
λ_{B}, r_{B}, h_{B}	Density, radius and height of human blockages
λ_{W}, L_{W}, θ_{W}, h_{W}	Density, length, orientation and height of wall blockages
$\kappa_{\mathrm{L,S}}$, $\kappa_{\mathrm{L,B}}(\cdot)$, $\kappa_{\mathrm{L,W}}(\cdot)$	LoS probability of the THz AP in the presence of only self-blockage, human blockers and wall blockers, respectively
$\sigma_{\varepsilon_{\mathrm{T}}}$, $\sigma_{\varepsilon_{\mathrm{U}}}$	THz/UE beam-steering error
χ_{R,x_i}, χ_{L,x_i}, χ_{N,x_i}	Small scale fading gain between the UE and an RF AP, a LoS THz AP or a NLoS THz AP, respectively, located at $\mathbf{x}_i$
d_{R,x_i}, d_{L,x_i}, d_{N,x_i}	Distance between UE and an RF AP, a LoS THz or a NLoS THz AP located at $\mathbf{x}_i$, respectively
d_{R}, d_{L}, d_{N}	Distance between the UE and its nearest RF AP, LoS THz AP or NLoS THz AP, respectively
x_{R}, x_{L}, x_{N}	Distance between the UE and its serving AP assuming that the UE is associating with an RF AP, a LoS THz AP or a NLoS THz AP, respectively
A_{R}, A_{L}, A_{N}	Probability of association with an RF AP, a LoS THz AP, or a NLoS THz AP, respectively
$P_{cov,\mathrm{R}}$, $P_{cov,\mathrm{L}}$, $P_{cov,\mathrm{N}}$	Conditional coverage probability given that the UE is associated with an RF AP, a LoS THz AP, or a NLoS THz AP, respectively
τ_{R}, τ_{L}, τ_{N}	Conditional average rate given that the UE is associated with an RF AP, a LoS THz AP, or a NLoS THz AP, respectively
P_{cov}, τ	Overall coverage probability and overall coverage rate
θ	SINR threshold

II. SYSTEM MODEL

In this section, we start by presenting the network model for the THz/RF coexisting indoor scenario, the different THz and RF channel models and the association policy.

A. Network Model

In this work, we model a downlink (DL) wireless network where a fixed number N_{A} of RF and THz APs are mounted on the ceiling of an indoor finite area $\mathcal{A}$ to serve the user equipments (UEs) as shown in Fig. 1. We consider the performance of a reference UE located at a fixed height h_{U} from the ground level and at an arbitrary location $\mathbf{v}_0$ from the origin $\mathbf{o} = (0, 0, 0)$ assumed to be in the same UE's plane.

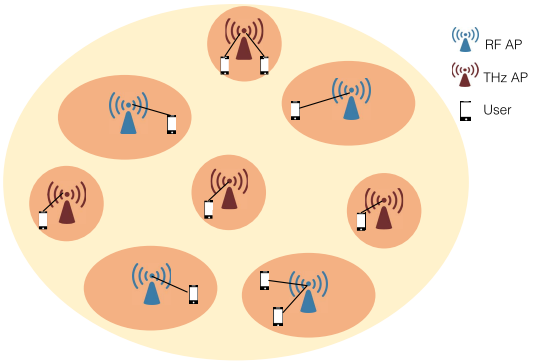

Fig. 1. Network architecture of the RF and THz finite coexisting network.

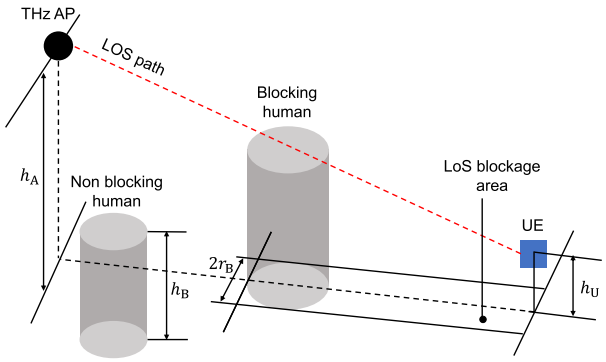

Fig. 2. Illustration of the human-blocking scenario for an AP-UE link.

The locations of the APs are modeled as a uniform binomial point process (BPP) $\Phi_{\mathrm{A}} \triangleq \{\mathbf{x}_i\}$, where $\mathbf{x}_i$ refers to the location of the i-th AP in the finite region $\mathcal{A} = \mathbf{b}(\mathbf{o'}, r_d)$ modeled as a disk of radius r_d centered around $\mathbf{o'} = (0, 0, h_{\mathrm{A}} - h_{\mathrm{U}})$, where h_{A} is the height of the APs from the ground level, and $h_{\mathrm{A}} - h_{\mathrm{U}}$ is the relative height with respect to the UE plane. As the BPP remains invariant with respect to the orientation of the axes, we can consider, without loss of generality, that the UE is located on the x-axis, i.e., the location of the UE is $\mathbf{v}_0 = (v_0, 0, 0)$, where $||\mathbf{v}_0|| = v_0 \in [0, r_d]$. A fraction δ_{T} of the APs are THz APs that transmit with the same power P_{T} while the remaining fraction of $(1 - \delta_{\mathrm{T}})$ are RF APs transmitting with a power P_{R}. From the UE's point of view, the set of APs is decomposed into two independent BPPs, i.e., $\Phi_{\mathrm{A}} = \Phi_{\mathrm{T}} \cup \Phi_{\mathrm{R}}$ where Φ_{T} and Φ_{R} denote the sets of THz and RF APs. Note here that δ_{T} should be chosen such that $\delta_{\mathrm{T}} N_{\mathrm{A}}$, which represents the total number of THz APs, is always an integer number. For the RF communication, the RF APs use omni-directional antennas to communicate with single antenna UEs. However, THz APs are equipped with dedicated antenna arrays that operate on the considered THz frequency to serve UEs with directional antennas. The UE evaluates the quality of the channel from each existing AP and associates to a specific AP according to the association rule described in Section II-D.

B. RF Channel Model

The RF communication is affected by a distance dependent large scale fading and a small scale multipath Rayleigh fading caused by the high density of humans and walls in the indoor environment. The fading assumption is motivated by the fact that, unlike the Rician fading, Rayleigh fading can effectively model indoor environments with high density of blockages while maintaining the tractability of mathematical analysis. Thus, the fading gain follows the exponential distribution with unit mean and the received power P^r_{R,x_i} from the i-th RF AP located at $\mathbf{x}_i$ is given by $P^r_{\mathrm{R},x_i} = P_{\mathrm{R}} \gamma_{\mathrm{R}} d^{-\alpha_{\mathrm{R}}}_{\mathrm{R},x_i} \chi_{\mathrm{R},x_i}$, where P_{R} is the RF AP transmit power, $\gamma_{\mathrm{R}} = \frac{c^2}{(4\pi f_{\mathrm{R}})^2}$, $d_{\mathrm{R},x_i} = ||\mathbf{x}_i - \mathbf{v}_0||$ is the distance from the UE to the i-th RF AP, α_{R} is the path loss exponent, χ_{R,x_i} is the gain of the small scale Rayleigh fading, f_{R} is the RF carrier frequency and $c = 3 \times 10^8$ m/s is the speed of light.

C. THz Channel Model

1) Blockage Model: THz propagation is highly affected by obstacles in the environment. The presence of these obstacles breaks the LoS connection and converts it to a NLoS connection. In this work, we assume that the blockage of a UE-AP link is caused by (i) the user itself, denoted as self-blockage, (ii) human blockers, and (iii) walls blockers. Self-blockage has a significant impact on THz communications and occurs when the UE blocks some of its surrounding APs even if they are within close proximity. The zone in which the APs are not blocked by self-blockage is determined by the self-blocking angle ω_{S}. The probability of having a LoS link between the UE and an AP in the existence of self-blockage is expressed as

$$\kappa_{\mathrm{L,S}} = \frac{2\pi - \omega_{\mathrm{S}}}{2\pi} = 1 - \frac{\omega_{\mathrm{S}}}{2\pi}. \tag{1}$$

In addition to self-blockage, humans bodies can cause significant losses on the THz propagation. We assume that human blockages are modeled as a random circle process of radius r_{B} and height h_{B}. Specifically, the bottom center of the cylinder characterizing a human blocker is modeled as a 2D homogeneous PPP of density λ_{B}. As a consequence of the high penetration loss of THz communication, if the LoS link is blocked by a human blocker, the UE can only communicate with the serving THz AP through reflected NLoS links. Fig. 2 shows the case when a human body blocks the AP-UE LoS link and convert it to a NLoS link. The probability of having a LoS connection between a THz AP located at a distance r from the UE in the existence of human blockers, denoted as $\kappa_{\mathrm{L,B}}(r)$, is estimated by the null probability of the human blockages PPP. Defining $\beta_{\mathrm{B}} = 2\lambda_{\mathrm{B}} r_{\mathrm{B}} \frac{|h_{\mathrm{B}} - h_{\mathrm{U}}|}{|h_{\mathrm{A}} - h_{\mathrm{U}}|}$, where h_{A} and h_{U} are the heights of the AP and the UE, the LoS probability in the presence of human blockers is given as [26]

$$\kappa_{\mathrm{L,B}}(r) = e^{-\beta_{\mathrm{B}} \sqrt{r^2 - (h_{\mathrm{A}} - h_{\mathrm{U}})^2}}, \tag{2}$$

where $\sqrt{r^2 - (h_{\mathrm{A}} - h_{\mathrm{U}})^2}$ is the Euclidean horizontal distance that separates the reference UE from the projection of the AP location on the UE plane.

To model the walls blockages in the indoor environment, we use a tractable boolean scheme of straight lines [35]. Specifically, the walls are modeled as line segments with length L_{W} and orientation θ_{W} where L_{W} is uniformly

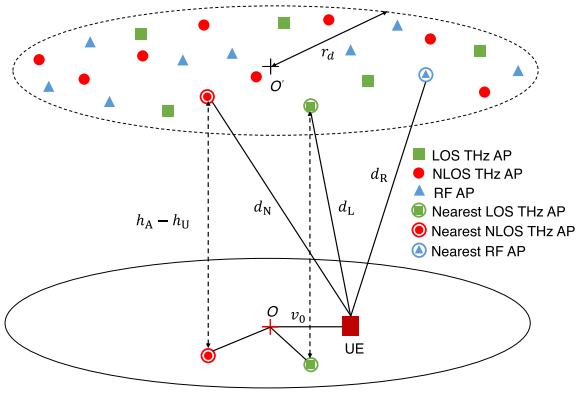

Fig. 3. BPP distribution of APs in the disk $\mathcal{A}$. The set of APs is divided into RF APs, LoS and NLoS THz APs.

distributed in $[L_{\mathrm{W}}^{\min}, L_{\mathrm{W}}^{\max}]$ and θ_{W} is a binary choice in $\{0, \frac{\pi}{2}\}$ with equal probability, respectively. Furthermore, we assume that the height of walls h_{W} is fixed and that they are at the same height of APs, i.e., $h_{\mathrm{W}} = h_{\mathrm{A}}$. The locations of the centers of the walls are modeled as a PPP with density λ_{W}. Thus, the LoS probability of an AP-UE link of length r in the presence of wall blockages only can be obtained by using the void probability of walls existing within the AP-UE link and is given as [28]

$$\kappa_{\mathrm{L,W}}(r) = e^{-\beta_{\mathrm{W}}\sqrt{r^2-(h_{\mathrm{A}}-h_{\mathrm{U}})^2}}, \tag{3}$$

where $\beta_{\mathrm{W}} = \frac{2\lambda_{\mathrm{W}}\mathbb{E}[L_{\mathrm{W}}]}{\pi}$ is the walls blockage parameter which is a function of the average size and the density of the walls.

Finally, the LoS probability for the link between the typical UE and an AP located at a distance r in the presence of self-blockage, human blockers and walls blockers is given as

$$\kappa_{\mathrm{L}}(r) = \kappa_{\mathrm{L,S}}\kappa_{\mathrm{L,B}}(r)\kappa_{\mathrm{L,W}}(r) = \kappa_{\mathrm{L,S}}e^{-\beta\sqrt{r^2-(h_{\mathrm{A}}-h_{\mathrm{U}})^2}}, \tag{4}$$

where $\beta = \beta_{\mathrm{B}} + \beta_{\mathrm{W}}$ is the blockage parameter which accounts for the human and walls blockers and $\kappa_{\mathrm{L,S}}$ is the non-self-blocking probability. The NLoS probability $\kappa_{\mathrm{N}}(r)$ reflects the probability that the link of length r separating the UE from the AP is in a NLoS condition due to large values of r or the existence of blockages and is given as

$$\kappa_{\mathrm{N}}(r) = 1 - \kappa_{\mathrm{L,S}}e^{-\beta\sqrt{r^2-(h_{\mathrm{A}}-h_{\mathrm{U}})^2}}. \tag{5}$$

Based on the considered channel model, the UE is exposed to either a LoS or a NLoS connection with any THz AP. Although this assumption becomes unrealistic in circumstances where APs are very close to each other and are likely to face the same LoS or NLoS situation, it can simplify the mathematical analysis significantly and leads as result to tractable analytical expressions. Thus, from the UE's perspective, the set of THz APs Φ_{T} will be divided into two disjoint subsets, i.e, $\Phi_{\mathrm{T}} = \Phi_{\mathrm{L}} \cup \Phi_{\mathrm{N}}$, where Φ_{L} and Φ_{N} represent the set of THz APs which are in LoS or NLoS situations with regard to the reference UE, respectively. This decomposition is done by mapping each point of Φ_{T} into one of the disjoint sets Φ_{L} and Φ_{N} with probabilities $\kappa_{\mathrm{L}}(r)$ and $\kappa_{\mathrm{N}}(r)$, respectively, where r represents the location of the AP. Fig. 3 shows a realization of the BPP of APs with the three subsets for RF, LoS THz and NLoS THz APs.

2) Propagation Model: THz communication is highly affected by the molecular absorption loss caused by water molecules in the atmosphere. Thus, large scale fading is modeled as a deterministic exponent power loss propagation model. Furthermore, since THz communication is very sensitive to the availability of LoS paths, the Rayleigh fading assumption is invalid and the small scale fading follows a Nakagami-m distribution instead. Nakagami-m fading has been used widely in the literature to model the small-scale fading of THz communications [26], [33], [36]. We use different path loss exponents and Nakagami-m parameters for THz LoS and NLoS transmissions (α_{L} and m_{L} for LoS links and α_{N} and m_{N} for NLoS links). Thus, the channel fading gain χ_{ξ,x_i}, $\xi \in \{\mathrm{L}, \mathrm{N}\}$, between the i-th THz AP located at $\mathbf{x}_i$ and the UE, follows Gamma distribution with shape and scale parameters given by $\left(m_\xi, \frac{1}{m_\xi}\right)$ and with a complementary cumulative distribution function (CCDF) given by

$$\bar{F}_{\chi_{\xi,x_i}}(x) = \sum_{k=0}^{m_\xi - 1} \frac{(m_\xi x)^k}{k!} \exp\left(-m_\xi x\right). \tag{6}$$

Considering probabilistic LoS and NLoS transmissions, the path loss between the reference UE and a THz AP can be expressed as $l_\xi(z) = \gamma_{\mathrm{T}} e^{-k_a(f_{\mathrm{T}})z} z^{-\alpha_\xi}$, where $\gamma_{\mathrm{T}} = \frac{c^2}{(4\pi f_{\mathrm{T}})^2}$, $k_a(f_{\mathrm{T}})$ is the molecular absorption coefficient, f_{T} is the THz carrier frequency and z is the distance between the UE and the considered AP, and where $\xi \in \{\mathrm{L}, \mathrm{N}\}$ depending on whether the THz AP has a LoS connection or NLoS connection with the UE. In THz communications, molecular absorption is remitted out of phase at the same frequencies initially absorbed, resulting in a source of noise dependent on operating frequencies, also known as molecular absorption noise [37], [38], [39]. The impact of such noise has been incorporated in reference stochastic geometry works in the literature [40], [41]. Nevertheless, we neglect absorption noise in our system-level analyses because its effect is secondary compared to interference [42].

3) Antenna Model: Directional antennas are usually used in THz communication because of the small antenna sizes which brought great potential for large multiple input multiple output (MIMO) arrays implementations [9], [43] to overcome the experienced large path and absorption losses. To account for the antenna array patterns of the THz APs and the UE, we use a sectored antenna model which has been extensively used in the literature [44], [45]. As such, the antenna gain can be expressed as

$$G_s(\varphi) = \begin{cases} G_s^{(\max)}, & |\varphi| \le \varphi_s \\ G_s^{(\min)}, & |\varphi| > \varphi_s \end{cases}, \tag{7}$$

where $\varphi \in [-\pi, \pi)$ represents the angle of boresight direction, $G_s^{(\max)}$, $G_s^{(\min)}$, and φ_s denote the main and side lobes gains and the beamwidth of the THz APs antennas and the UEs antennas operating in the THz band ($s \in \{\mathrm{T}, \mathrm{U}\}$), respectively.

When the UE chooses to associate with a THz AP, both the UE and AP steer their directional antennas to increase the directionality gain. In the absence of beam-steering errors, the UE can benefit from the gains of the main lobes of its antenna and the antenna of the THz AP. In this case, the directionality

TABLE II
PROBABILITY MASS FUNCTION OF THE THZ DIRECTIONALITY GAIN

k	1	2	3	4
G_k	$G_{\mathrm{T}}^{\max}G_{\mathrm{U}}^{\max}$	$G_{\mathrm{T}}^{\max}G_{\mathrm{U}}^{\min}$	$G_{\mathrm{T}}^{\min}G_{\mathrm{U}}^{\max}$	$G_{\mathrm{T}}^{\min}G_{\mathrm{U}}^{\min}$
$p_{k,0}$	$F_{\lvert\varepsilon_{\mathrm{T}}\rvert}(\frac{\varphi_{\mathrm{T}}}{2})F_{\lvert\varepsilon_{\mathrm{U}}\rvert}(\frac{\varphi_{\mathrm{U}}}{2})$	$F_{\lvert\varepsilon_{\mathrm{T}}\rvert}(\frac{\varphi_{\mathrm{T}}}{2})\bar{F}_{\lvert\varepsilon_{\mathrm{U}}\rvert}(\frac{\varphi_{\mathrm{U}}}{2})$	$\bar{F}_{\lvert\varepsilon_{\mathrm{T}}\rvert}(\frac{\varphi_{\mathrm{T}}}{2})F_{\lvert\varepsilon_{\mathrm{U}}\rvert}(\frac{\varphi_{\mathrm{U}}}{2})$	$\bar{F}_{\lvert\varepsilon_{\mathrm{T}}\rvert}(\frac{\varphi_{\mathrm{T}}}{2})\bar{F}_{\lvert\varepsilon_{\mathrm{U}}\rvert}(\frac{\varphi_{\mathrm{U}}}{2})$
p_k	$v_{\mathrm{T}}v_{\mathrm{U}}$	$v_{\mathrm{T}}(1-v_{\mathrm{U}})$	$(1-v_{\mathrm{T}})v_{\mathrm{U}}$	$(1-v_{\mathrm{T}})(1-v_{\mathrm{U}})$

gain on the desired link is given by $G_{\mathrm{T},0} = G_{\mathrm{T}}^{\max}G_{\mathrm{U}}^{\max}$. However, achieving perfect alignment is not always feasible as it requires extremely narrow beams and further processing at both sides. To account for the beam-steering error on the THz-UE connection, we use the model proposed in [46], so let ε_{T} and ε_{U} denote the added beam-steering errors on the THz AP and the UE respectively. We assume that ε_{T} and ε_{U} are independent and Gaussian distributed with zero mean and variances $\sigma^2_{\varepsilon_{\mathrm{T}}}$ and $\sigma^2_{\varepsilon_{\mathrm{U}}}$, respectively. Furthermore, we assume that ε_{T} and ε_{U} are symmetrically distributed around the error-free beam-steering angles. Thus, $|\varepsilon_s|$ ($s \in \{\mathrm{T},\mathrm{U}\}$) has a half-normal distribution with cumulative distribution function (CDF) $F_{|\varepsilon_s|}(x) = \mathrm{erf}\left(\frac{x}{\sqrt{2}\sigma_{\varepsilon_s}}\right)$, where $\mathrm{erf}(\cdot)$ is the error function.

As the antenna gain of the THz AP and the UE is a discrete random variable that can take only two values as given in (7), the corresponding probability mass function (PMF) in the presence of beam-steering errors can be expressed as [46]

$$f_{G_s}(g) = F_{|\varepsilon_s|}\left(\frac{\varphi_s}{2}\right)\delta\left(g - G_s^{\max}\right) + \bar{F}_{|\varepsilon_s|}\left(\frac{\varphi_s}{2}\right)\delta\left(g - G_s^{\min}\right), \quad (8)$$

where $\delta(\cdot)$ denotes the Dirac delta function and $\bar{F}_{|\varepsilon_s|}(x) = \big(1 - F_{|\varepsilon_s|}(x)\big)$. Accordingly, the directionality gain on the intended link $G_{\mathrm{T},0}$ is also a discrete random variable with a range of possible values G_k ($k \in \{1,2,3,4\}$) and corresponding probabilities $p_{k,0}$ given in Table II.

As the UE associates with a THz AP, the remaining THz APs will act as interferers that can affect the THz connection. However, the antennas of the interfering THz APs are not necessarily steered towards the reference UE that can receive interference from either the main lobe or the side lobe of the directional antenna. To account for the THz interference, we consider that the steering angles between the i-th THz AP located at $\mathbf{x}_i$ and the UE are uniformly distributed over $[0, 2\pi]$. Thus, the directionality gain G_{T,x_i} is a discrete random variable that can take four values G_k, ($k \in \{1,2,3,4\}$) with probabilities p_k as given in Table II, where $v_{\mathrm{T}} = \frac{\varphi_{\mathrm{T}}}{2\pi}$ and $v_{\mathrm{U}} = \frac{\varphi_{\mathrm{U}}}{2\pi}$, φ_{T} and φ_{U} are the beamwidth for the THz APs and the UEs antennas, respectively. The received power at the reference UE from the i-th THz AP placed at $\mathbf{x}_i$ is given as $P^r_{\xi,x_i} = P_{\mathrm{T}}\gamma_{\mathrm{T}}G_{\mathrm{T},x_i}e^{-k_a(f_{\mathrm{T}})d_{\xi,x_i}}d^{-\alpha_\xi}_{\xi,x_i}\chi_{\xi,x_i}$, where $\xi \in \{\mathrm{L},\mathrm{N}\}$ specifies whether the THz AP located at $\mathbf{x}_i$ has a LoS or a NLoS connection with the reference UE. χ_{ξ,x_i} is the small scale Nakagami fading, $\gamma_{\mathrm{T}} = \frac{c^2}{(4\pi f_{\mathrm{T}})^2}$, P_{T} is the THz AP transmit power, $d_{\xi,x_i} = ||\mathbf{x}_i - \mathbf{v}_0||$ is the distance from the UE to the i-th THz AP, α_ξ is the path loss exponent, f_{T} is the THz carrier frequency.

D. Association Policy and SINR

In this paper, we assume that the association decision is taken by referring to long term evaluation of the channel instead of short term metrics. The UE has three association options: an RF AP, a LoS THz AP or a NLoS THz AP depending on the strongest averaged biased received signal power (BRSP). Here, biased association is considered to avoid under-utilization of THz APs. Note here that the nearest AP is not necessarily the AP that provides the strongest received power because of the difference in path-loss parameters, transmit powers and antenna configurations. However, within a specific set of APs, i.e., within each set of RF, LoS THz and NLoS THz APs, the aforementioned parameters are the same for all connections. Thus, for a particular set, the nearest AP has a larger average received power than that offered by all the remaining APs in that set. As result, the serving AP is always the closest RF, LoS THz or NLoS THz AP. According to the considered association rule and the assumptions that $\mathbb{E}[\chi_{\mathrm{R},x_i}] = \mathbb{E}[\chi_{\mathrm{L},x_i}] = \mathbb{E}[\chi_{\mathrm{N},x_i}] = 1$, the serving AP is given as $\mathrm{argmax}\{P_{\mathrm{R}}\gamma_{\mathrm{R}}d_{\mathrm{R}}^{-\alpha_{\mathrm{R}}}, B_{\mathrm{T}}P_{\mathrm{T}}\gamma_{\mathrm{T}}G_{\mathrm{T},0}^{(\mathrm{mean})}e^{-k_a(f_{\mathrm{T}})d_{\mathrm{L}}}d_{\mathrm{L}}^{-\alpha_{\mathrm{L}}}, B_{\mathrm{T}}P_{\mathrm{T}}\gamma_{\mathrm{T}}G_{\mathrm{T},0}^{(\mathrm{mean})}e^{-k_a(f_{\mathrm{T}})d_{\mathrm{N}}}d_{\mathrm{N}}^{-\alpha_{\mathrm{N}}}\}$, where $d_{\mathrm{R}} = \min_{\forall\mathbf{x}_i\in\Phi_{\mathrm{R}}} d_{\mathrm{R},x_i}$, $d_{\mathrm{L}} = \min_{\forall\mathbf{x}_i\in\Phi_{\mathrm{L}}} d_{\mathrm{L},x_i}$, and $d_{\mathrm{N}} = \min_{\forall\mathbf{x}_i\in\Phi_{\mathrm{N}}} d_{\mathrm{N},x_i}$ are the distances from the UE to the nearest RF, LoS THz and NLoS THz APs. $G_{\mathrm{T},0}^{(\mathrm{mean})} = \sum_{k=1}^{4} p_{k,0}G_k$ is the average directionality gain on the desired THz link, where $p_{k,0}$ and G_k are given in Table II. B_{T} is the THz bias parameter. For $B_{\mathrm{T}} > 1$, the UE is encouraged to associate more with THz APs. For $0 \le B_{\mathrm{T}} < 1$, association with RF APs is promoted.

As the objective of this work is to assess the DL performance of a coexisting RF/THz network, the main performance metrics used are the DL coverage probability and the average rate. To this end, we define the coverage probability, P_{cov}, as the probability that the SINR at the UE exceeds a threshold θ. When the UE associates with an RF AP, the SINR can be formulated as:

$$\mathrm{SINR}_{\mathrm{R}} = \frac{P_{\mathrm{R}}\gamma_{\mathrm{R}}x_{\mathrm{R}}^{-\alpha_{\mathrm{R}}}\chi_{\mathrm{R},0}}{I_{\mathrm{R}} + \sigma^2_{\mathrm{R}}}, \quad (9)$$

where $\chi_{\mathrm{R},0}$ is the small scale fading experienced by the UE on the desired link, x_{R} is the distance separating the UE from the serving RF AP, σ^2_{R} is the noise variance and I_{R} is the interference at the reference UE from other RF APs and is given by

$$I_{\mathrm{R}} = \sum_{\mathbf{x}_i\in\Phi_{\mathrm{R}}/x_{\mathrm{R}}} P_{\mathrm{R}}\gamma_{\mathrm{R}}d_{\mathrm{R},x_i}^{-\alpha_{\mathrm{R}}}\chi_{\mathrm{R},x_i}, \quad (10)$$

where d_{R,x_i} is the distance separating the interfering RF AP located at $\mathbf{x}_i$ from the reference UE.

Similarly, the SINR of the reference UE when associating with a THz AP is given as

$$\mathrm{SINR}_{\xi} = \frac{P_{\mathrm{T}}\gamma_{\mathrm{T}}G_{\mathrm{T},0}e^{-k_a(f_{\mathrm{T}})x_\xi}x_\xi^{-\alpha_\xi}\chi_{\xi,0}}{I_\xi + \sigma^2_{\mathrm{T}}}, \quad (11)$$

where $\xi \in \{\mathrm{L},\mathrm{N}\}$ indicates if the serving AP is a LoS or a NLoS AP, x_ξ is the distance that separates the UE from the serving THz AP, $G_{\mathrm{T},0}$ is the directionality gain which

has a PMF given in Table II, $\chi_{\xi,0}$ denotes the small-scale fading, and σ_{T}^2 is the thermal noise. Here, I_ξ is the aggregate interference from the remaining LoS and NLoS THz APs. Thus, I_ξ is given as

$$I_\xi = \sum_{\mathbf{x}_i \in \Phi_\xi / x_\xi} P_{\mathrm{T}} \gamma_{\mathrm{T}} G_{\mathrm{T},x_i} e^{-k_a(f_{\mathrm{T}}) d_{\xi,x_i}} d_{\xi,x_i}^{-\alpha_\xi} \chi_{\xi,x_i} + \sum_{\mathbf{x}_i \in \Phi_{\bar{\xi}}} P_{\mathrm{T}} \gamma_{\mathrm{T}} G_{\mathrm{T},x_i} e^{-k_a(f_{\mathrm{T}}) d_{\bar{\xi},x_i}} d_{\bar{\xi},x_i}^{-\alpha_{\bar{\xi}}} \chi_{\bar{\xi},x_i}, \quad (12)$$

where $\bar{\xi} = \mathrm{N}$ if $\xi = \mathrm{L}$ and $\bar{\xi} = \mathrm{L}$ if $\xi = \mathrm{N}$, G_{T,x_i} is the directionality gain between the i-th interfering THz AP and the reference UE, d_{ξ,x_i} and $d_{\bar{\xi},x_i}$ denote the distances between the THz AP located at $\mathbf{x}_i$ and the reference UE for LoS and NLoS transmissions.

III. Association Probabilities and Serving Distance Distributions

Referring to the considered association policy, the UE can be served by either a LoS THz AP (denoted hereafter as L-THz AP), a NLoS THz AP (denoted hereafter as N-THz AP) or an RF AP, respectively. To account for the three association events, we divide the sample space into three disjoint events, C_Q, $Q = \{\mathrm{L}, \mathrm{N}, \mathrm{R}\}$, representing associating with a L-THz AP, a N-THz AP or an RF AP, respectively. Now, the association probability A_Q is defined as the probability of occurrence of the disjoint event C_Q, $Q = \{\mathrm{L}, \mathrm{N}, \mathrm{R}\}$. We start this section by presenting first relevant distance distributions and exclusion regions expressions. These expressions are needed to obtain the association probabilities and the Laplace transforms of the interference powers.

A. Relevant Distance Distributions and Exclusion Regions

As the APs are distributed according to a BPP in a finite disk $\mathcal{A}$ of radius r_d, the probability density function (PDF) of the distance between an AP located at $\mathbf{x}_i$ and the reference UE at $\mathbf{v}_0 = (v_0, 0, 0)$ is given by [47, eq. (7)]

$$f_{\mathrm{Z}}(z) = \begin{cases} f_{\mathrm{Z}_1}(z) = \frac{2z}{r_d^2}, & z_l \le z \le z_m \\ f_{\mathrm{Z}_2}(z) = \frac{2z}{\pi r_d^2} \arccos\left(\frac{z^2 + v_0^2 - r_d^2 - (h_{\mathrm{A}} - h_{\mathrm{U}})^2}{2 v_0 \sqrt{z^2 - (h_{\mathrm{A}} - h_{\mathrm{U}})^2}} \right), & z_m \le z \le z_p, \end{cases} \quad (13)$$

where $z_l = h_{\mathrm{A}} - h_{\mathrm{U}}$, $z_m = \sqrt{(r_d - v_0)^2 + (h_{\mathrm{A}} - h_{\mathrm{U}})^2}$, $z_p = \sqrt{(r_d + v_0)^2 + (h_{\mathrm{A}} - h_{\mathrm{U}})^2}$, and h_{A} and h_{U} are the heights at which the APs and the reference UE are deployed.

From the system model, we note that all APs are at least a distance $h_{\mathrm{A}} - h_{\mathrm{U}}$ from the reference UE. Now, when the UE associates with an AP according to the BRSP policy, this creates an exclusion region on the interfering APs and therefore on the positions of these APs in each set. This happens for each association event, i.e, for each event, C_Q, $Q = \{\mathrm{L}, \mathrm{N}, \mathrm{R}\}$. The following remarks spell out the exclusion regions on the locations of the APs for each association type.

Remark 1 (Exclusion regions for THz AP association): If the UE associates with a ξ-THz AP ($\xi \in \{\mathrm{L}, \mathrm{N}\}$) located at a distance r, the nearest RF AP and $\bar{\xi}$-THz AP are located further than $E_{\xi\mathrm{R}}(r)$ and $E_{\xi\bar{\xi}}(r)$, respectively, given by

$$E_{\xi\mathrm{R}}(r) = \begin{cases} h_{\mathrm{A}} - h_{\mathrm{U}}, & h_{\mathrm{A}} - h_{\mathrm{U}} \le r < h_{\xi\mathrm{R}} \\ \left(\frac{P_{\mathrm{R}} \gamma_{\mathrm{R}}}{B_{\mathrm{T}} P_{\mathrm{T}} \gamma_{\mathrm{T}} G_{\mathrm{T},0}^{(\mathrm{mean})}} \right)^{\frac{1}{\alpha_{\mathrm{R}}}} e^{\frac{k_a(f_{\mathrm{T}})}{\alpha_{\mathrm{R}}} r} r^{\frac{\alpha_\xi}{\alpha_{\mathrm{R}}}}, & r \ge h_{\xi\mathrm{R}}, \end{cases} \quad (14)$$

$$E_{\xi\bar{\xi}}(r) = \begin{cases} h_{\mathrm{A}} - h_{\mathrm{U}}, & h_{\mathrm{A}} - h_{\mathrm{U}} \le r < h_{\xi\bar{\xi}} \\ \frac{\alpha_{\bar{\xi}}}{k_a(f_{\mathrm{T}})} \mathcal{W}\left[\frac{k_a(f_{\mathrm{T}})}{\alpha_{\bar{\xi}}} e^{\frac{k_a(f_{\mathrm{T}})}{\alpha_{\bar{\xi}}} r} r^{\frac{\alpha_\xi}{\alpha_{\bar{\xi}}}} \right] & r \ge h_{\xi\bar{\xi}}, \end{cases} \quad (15)$$

where $\mathcal{W}[\cdot]$ is the Lambert W-function, $h_{\xi\mathrm{R}} = \frac{\alpha_\xi}{k_a(f_{\mathrm{T}})} \mathcal{W}\left[\frac{k_a(f_{\mathrm{T}})}{\alpha_\xi} \left(\frac{B_{\mathrm{T}} P_{\mathrm{T}} \gamma_{\mathrm{T}} G_{\mathrm{T},0}^{(\mathrm{mean})}}{P_{\mathrm{R}} \gamma_{\mathrm{R}}} \right)^{\frac{1}{\alpha_\xi}} (h_{\mathrm{A}} - h_{\mathrm{U}})^{\frac{\alpha_{\mathrm{R}}}{\alpha_\xi}} \right]$, $h_{\xi\bar{\xi}} = \frac{\alpha_\xi}{k_a(f_{\mathrm{T}})} \mathcal{W}\left[\frac{k_a(f_{\mathrm{T}})}{\alpha_\xi} e^{\frac{k_a(f_{\mathrm{T}})}{\alpha_\xi}(h_{\mathrm{A}} - h_{\mathrm{U}})} (h_{\mathrm{A}} - h_{\mathrm{U}})^{\frac{\alpha_{\bar{\xi}}}{\alpha_\xi}} \right]$, $\bar{\xi} = \mathrm{N}$ if $\xi = \mathrm{L}$ and $\bar{\xi} = \mathrm{L}$ if $\xi = \mathrm{N}$.

Proof: The biased average received power from a L-THz AP located at r is given as $P_{\mathrm{L}}^r = B_{\mathrm{T}} P_{\mathrm{T}} \gamma_{\mathrm{T}} G_{\mathrm{T},0}^{(\mathrm{mean})} e^{-k_a(f) r} r^{-\alpha_{\mathrm{L}}}$. As the UE associates to the AP that provides the strongest BRSP, the distance separating the closest RF AP from the UE $E_{\mathrm{LR}}(r)$ is obtained by solving the equation $B_{\mathrm{T}} P_{\mathrm{T}} \gamma_{\mathrm{T}} G_{\mathrm{T},0}^{(\mathrm{mean})} e^{-k_a(f) r} r^{-\alpha_{\mathrm{L}}} = P_{\mathrm{R}} \gamma_{\mathrm{R}} E_{\mathrm{LR}}^{-\alpha_{\mathrm{R}}}(r)$. Similarly, $E_{\mathrm{LN}}(r)$ can be found by solving the equation $B_{\mathrm{T}} P_{\mathrm{T}} \gamma_{\mathrm{T}} G_{\mathrm{T},0}^{(\mathrm{mean})} e^{-k_a(f) r} r^{-\alpha_{\mathrm{L}}} = B_{\mathrm{T}} P_{\mathrm{T}} \gamma_{\mathrm{T}} G_{\mathrm{T},0}^{(\mathrm{mean})} e^{-k_a(f) E_{\mathrm{LN}}(r)} E_{\mathrm{LN}}^{-\alpha_{\mathrm{L}}}(r)$. The expressions of $E_{\mathrm{LR}}(r)$ and $E_{\mathrm{LN}}(r)$ hold if $h_{\mathrm{LR}} > h_{\mathrm{A}} - h_{\mathrm{U}}$ and $h_{\mathrm{LN}} > h_{\mathrm{A}} - h_{\mathrm{U}}$. Otherwise, these expressions simplify to the second term of the piece-wise functions for $r \ge h_{\mathrm{A}} - h_{\mathrm{U}}$. The expressions of the exclusion regions $E_{\mathrm{NR}}(r)$ and $E_{\mathrm{NL}}(r)$ when the UE associates with a N-THz AP are obtained following a similar proof, thus omitted. ■

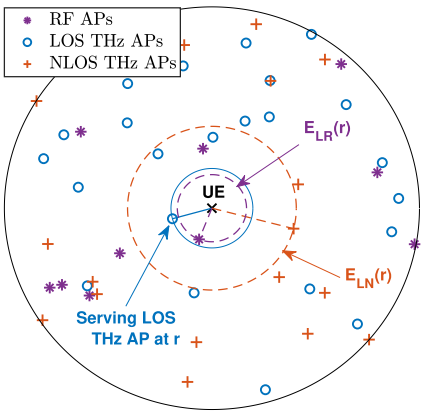

Fig. 4. Exclusion regions $E_{\mathrm{LN}}(r)$ and $E_{\mathrm{LR}}(r)$ on the N-THz and RF APs when the UE associates with a L-THz AP at r.

Fig. 4 shows a top view of the exclusion regions $E_{\mathrm{LN}}(r)$ and $E_{\mathrm{LR}}(r)$ created on the positions of the nearest N-THz and RF AP and as result on all the N-THz and RF APs, when the UE is associated with a L-THz AP located at a distance r in the

finite area. We can note that the serving L-THz AP is not the closest AP to the UE according to the BRSP association policy.

Remark 2 (Exclusion regions for RF AP association): If the UE associates to an RF AP located at a distance r, the nearest L*-THz and* N*-THz APs are located further than $E_{\mathrm{RL}}(r)$ and $E_{\mathrm{RN}}(r)$, respectively, given by*

$$E_{\mathrm{RL}}(r) = \begin{cases} h_{\mathrm{A}}-h_{\mathrm{U}}, & h_{\mathrm{A}}-h_{\mathrm{U}} \le r < h_{\mathrm{RL}} \\ \frac{\alpha_{\mathrm{L}}}{k_a(f_{\mathrm{T}})}\mathcal{W}\left[\frac{k_a(f_{\mathrm{T}})}{\alpha_{\mathrm{L}}}\left(\frac{B_{\mathrm{T}}P_{\mathrm{T}}\gamma_{\mathrm{T}}G_{\mathrm{T},0}^{(\mathrm{mean})}}{P_{\mathrm{R}}\gamma_{\mathrm{R}}}\right)^{\frac{1}{\alpha_{\mathrm{L}}}} r^{\frac{\alpha_{\mathrm{R}}}{\alpha_{\mathrm{L}}}}\right], & r \ge h_{\mathrm{RL}}, \end{cases} \tag{16}$$

$$E_{\mathrm{RN}}(r) = \begin{cases} h_{\mathrm{A}}-h_{\mathrm{U}}, & h_{\mathrm{A}}-h_{\mathrm{U}} \le r < h_{\mathrm{RN}} \\ \frac{\alpha_{\mathrm{N}}}{k_a(f_{\mathrm{T}})}\mathcal{W}\left[\frac{k_a(f_{\mathrm{T}})}{\alpha_{\mathrm{N}}}\left(\frac{B_{\mathrm{T}}P_{\mathrm{T}}\gamma_{\mathrm{T}}G_{\mathrm{T},0}^{(\mathrm{mean})}}{P_{\mathrm{R}}\gamma_{\mathrm{R}}}\right)^{\frac{1}{\alpha_{\mathrm{N}}}} r^{\frac{\alpha_{\mathrm{R}}}{\alpha_{\mathrm{N}}}}\right], & r \ge h_{\mathrm{RN}}, \end{cases} \tag{17}$$

where $\mathcal{W}[\cdot]$ is the Lambert W-function, $h_{\mathrm{RL}} = \left(\frac{P_{\mathrm{R}}\gamma_{\mathrm{R}}}{B_{\mathrm{T}}P_{\mathrm{T}}\gamma_{\mathrm{T}}G_{\mathrm{T},0}^{(\mathrm{mean})}}\right)^{\frac{1}{\alpha_{\mathrm{R}}}} e^{\frac{k_a(f_{\mathrm{T}})}{\alpha_{\mathrm{R}}}(h_{\mathrm{A}}-h_{\mathrm{U}})}(h_{\mathrm{A}}-h_{\mathrm{U}})^{\frac{\alpha_{\mathrm{L}}}{\alpha_{\mathrm{R}}}}$ and $h_{\mathrm{RN}} = \left(\frac{P_{\mathrm{R}}\gamma_{\mathrm{R}}}{B_{\mathrm{T}}P_{\mathrm{T}}\gamma_{\mathrm{T}}G_{\mathrm{T},0}^{(\mathrm{mean})}}\right)^{\frac{1}{\alpha_{\mathrm{R}}}} e^{\frac{k_a(f_{\mathrm{T}})}{\alpha_{\mathrm{R}}}(h_{\mathrm{A}}-h_{\mathrm{U}})}(h_{\mathrm{A}}-h_{\mathrm{U}})^{\frac{\alpha_{\mathrm{N}}}{\alpha_{\mathrm{R}}}}$.

Proof: The proof is similar to that of (14) and (15) and therefore is omitted. ∎

Next, we derive the association probabilities and the corresponding serving distance distributions for the three different association events.

B. Association Probabilities

In the coexisting RF/THz network, the UE associates with an RF AP, a L-THz AP or a N-THz AP according to the maximum BRSP association policy. The corresponding association probabilities A_{L}, A_{N} and A_{R} are presented in Lemma 1.

Lemma 1 (Association probabilities): The probabilities that the reference UE is served by a L*-THz AP, a* N*-THz AP and an RF AP, denoted as the LoS THz association probability A_{L}, the NLoS THz association probability A_{N} and the RF association probability A_{R}, respectively, are calculated as*

$$A_{\xi} = \delta_{\mathrm{T}}N_{\mathrm{A}}\int_{z_l}^{z_p} f_{\mathrm{Z}}(r)\kappa_{\xi}(r)\left(\int_{E_{\xi\mathrm{R}}(r)}^{z_p} f_{\mathrm{Z}}(z)\mathrm{d}z\right)^{(1-\delta_{\mathrm{T}})N_{\mathrm{A}}} \times\left(\int_{r}^{z_p} f_{\mathrm{Z}}(z)\kappa_{\xi}(z)\mathrm{d}z+\int_{E_{\xi\bar{\xi}}(r)}^{z_p} f_{\mathrm{Z}}(z)\kappa_{\bar{\xi}}(z)\mathrm{d}z\right)^{\delta_{\mathrm{T}}N_{\mathrm{A}}-1}\mathrm{d}r, \tag{18}$$

$$A_{\mathrm{R}} = (1-\delta_{\mathrm{T}})N_{\mathrm{A}}\int_{z_l}^{z_p} f_{\mathrm{Z}}(r)\left(\int_{r}^{z_p} f_{\mathrm{Z}}(z)\mathrm{d}z\right)^{(1-\delta_T)N_{\mathrm{A}}-1} \times\left(\int_{E_{\mathrm{RL}}(r)}^{z_p} f_{\mathrm{Z}}(z)\kappa_{\mathrm{L}}(z)\mathrm{d}z+\int_{E_{\mathrm{RN}}(r)}^{z_p} f_{\mathrm{Z}}(z)\kappa_{\mathrm{N}}(z)\mathrm{d}z\right)^{\delta_T N_{\mathrm{A}}}\mathrm{d}r, \tag{19}$$

where $\xi \in \{\mathrm{L},\mathrm{N}\}$ indicates if the AP is a L*-THz or a* N*-THz AP, $\bar{\xi} = \mathrm{N}$ if $\xi = \mathrm{L}$ and $\bar{\xi} = \mathrm{L}$ if $\xi = \mathrm{N}$, $f_{\mathrm{Z}}(z)$ is the PDF of the distance from the UE to any AP given in (13), $\kappa_{\mathrm{L}}(\cdot)$ and $\kappa_{\mathrm{N}}(\cdot)$ are the LoS and NLoS probabilities given in (4) and (5), respectively. $E_{\xi\mathrm{R}}(r)$, $E_{\xi\bar{\xi}}(r)$, $E_{\mathrm{RL}}(r)$, and $E_{\mathrm{RN}}(r)$ represent the exclusion regions on the locations of the interfering APs for each association event and can be found in (14), (15), (17) and (17), respectively.*

Proof: See Appendix A for the derivation of A_{L} given in (18). The proofs related to A_{N} and A_{R} are omitted as they are similar. ∎

Note here that the probability that the UE is associated with a THz AP is $A_{\mathrm{T}} = A_{\mathrm{L}} + A_{\mathrm{N}}$ and that $A_{\mathrm{T}} + A_{\mathrm{R}} = 1$.

C. Serving Distance Distributions

In this subsection, we derive the conditional distance distributions separating the UE from the serving L-THz, N-THz and RF APs. The derived distance distributions are provided in Lemma 2.

Lemma 2 (Serving distance distributions): The PDFs of the distances separating the location of the UE from its serving AP, given that this serving AP is a L*-THz AP, a* N*-THz AP or an RF AP and denoted by $f_{X_{\mathrm{L}}}(\cdot)$, $f_{X_{\mathrm{N}}}(\cdot)$ and $f_{X_{\mathrm{R}}}(\cdot)$, respectively, can be obtained as*

$$f_{X_{\xi}}(x_{\xi}) = \frac{\delta_{\mathrm{T}}N_{\mathrm{A}}}{A_{\xi}} f_{\mathrm{Z}}(x_{\xi})\kappa_{\xi}(x_{\xi})\left(\int_{E_{\xi\mathrm{R}}(x_{\xi})}^{z_p} f_{\mathrm{Z}}(z)\mathrm{d}z\right)^{(1-\delta_{\mathrm{T}})N_{\mathrm{A}}} \times\left(\int_{x_{\xi}}^{z_p} f_{\mathrm{Z}}(z)\kappa_{\xi}(z)\mathrm{d}z+\int_{E_{\xi\bar{\xi}}(x_{\xi})}^{z_p} f_{\mathrm{Z}}(z)\kappa_{\bar{\xi}}(z)\mathrm{d}z\right)^{\delta_{\mathrm{T}}N_{\mathrm{A}}-1}, \tag{20}$$

$$f_{X_{\mathrm{R}}}(x_{\mathrm{R}}) = \frac{(1-\delta_{\mathrm{T}})N_{\mathrm{A}}}{A_{\mathrm{R}}} f_{\mathrm{Z}}(x_{\mathrm{R}})\left(\int_{x_{\mathrm{R}}}^{z_p} f_{\mathrm{Z}}(z)\mathrm{d}z\right)^{(1-\delta_{\mathrm{T}})N_{\mathrm{A}}-1} \times\left(\int_{E_{\mathrm{RL}}(x_{\mathrm{R}})}^{z_p} f_{\mathrm{Z}}(z)\kappa_{\mathrm{L}}(z)\mathrm{d}z+\int_{E_{\mathrm{RN}}(x_{\mathrm{R}})}^{z_p} f_{\mathrm{Z}}(z)\kappa_{\mathrm{N}}(z)\mathrm{d}z\right)^{\delta_{\mathrm{T}}N_{\mathrm{A}}}, \tag{21}$$

where $\bar{\xi} = \mathrm{N}$ if $\xi = \mathrm{L}$ and $\bar{\xi} = \mathrm{L}$ if $\xi = \mathrm{N}$, $f_{\mathrm{Z}}(\cdot)$, $\kappa_{\mathrm{L}}(\cdot)$ and $\kappa_{\mathrm{N}}(\cdot)$ are provided in (13), (4) and (5). A_{L}, A_{N} and A_{R} are the association probabilities given in (18) and (19), respectively.

Proof: The distribution of the distance separating the UE from the serving LoS THz AP x_{L} is equivalent to the distribution of d_{L}, where d_{L} is the distance to the closest LoS THz AP, given that the UE associates with a LoS THz AP (i.e. given that the event C_{L} occurs). Thus, the complementary cumulative distribution function (CCDF) of X_{L} can be obtained as

$$\bar{F}_{X_{\mathrm{L}}}(x_{\mathrm{L}}) = \mathbb{P}\left[d_{\mathrm{L}} > x_{\mathrm{L}} | C_{\mathrm{L}}\right] = \frac{\mathbb{P}\left[d_{\mathrm{L}} > x_{\mathrm{L}}, C_{\mathrm{L}}\right]}{\mathbb{P}\left[C_{\mathrm{L}}\right]}, \tag{22}$$

where $\mathbb{P}\left[C_{\mathrm{L}}\right] = A_{\mathrm{L}}$ is given in (18). For the case when the UE chooses to associate with a LoS THz APs at distance r, any of the remaining APs is either a LoS THz AP located at a greater distance than r, a NLoS THz AP located at a greater distance than $E_{\mathrm{LN}}(r)$ or an RF AP located further than $E_{\mathrm{LR}}(r)$. As the N_{A} APs are independent and identically

distributed (i.i.d) after conditioning on the location of the UE, and given that a fraction δ_{T} of these APs are THz APs, the numerator of (22) is given as

$$\begin{aligned}&\mathbb{P}\left[d_{\mathrm{L}} > x_{\mathrm{L}}, C_{\mathrm{L}}\right]\\ &= \delta_{\mathrm{T}} N_{\mathrm{A}} \int_{x_{\mathrm{L}}}^{z_p} f_{\mathrm{Z}}(r)\kappa_{\mathrm{L}}(r) \left(\int_{E_{\mathrm{LR}(r)}}^{z_p} f_{\mathrm{Z}}(z)\mathrm{d}z\right)^{(1-\delta_{\mathrm{T}})N_{\mathrm{A}}}\\ &\quad \left(\int_{r}^{z_p} f_{\mathrm{Z}}(z)\kappa_{\mathrm{L}}(z)\mathrm{d}z + \int_{E_{\mathrm{LN}(r)}}^{z_p} f_{\mathrm{Z}}(z)\kappa_{\mathrm{N}}(z)\mathrm{d}z\right)^{\delta_{\mathrm{T}} N_{\mathrm{A}}-1} \mathrm{d}r,\end{aligned} \tag{23}$$

where $f_{\mathrm{Z}}(\cdot)$, $\kappa_{\mathrm{L}}(\cdot)$ and $\kappa_{\mathrm{N}}(\cdot)$ are given in (13), (4) and (5), respectively. $E_{\mathrm{LR}}(\cdot)$ and $E_{\mathrm{LN}}(\cdot)$ are the exclusion regions on the locations of the remaining APs and are given in (14) and (15), respectively. The cumulative distribution function (CDF) of X_{L} is $F_{X_{\mathrm{L}}}(x_{\mathrm{L}}) = 1 - \bar{F}_{X_{\mathrm{L}}}(x_{\mathrm{L}})$ and the PDF $f_{X_{\mathrm{L}}}(x_{\mathrm{L}}) = \frac{\mathrm{d}F_{X_{\mathrm{L}}}(x_{\mathrm{L}})}{\mathrm{d}x_{\mathrm{L}}}$ is given as in (21). The proofs related to $f_{X_{\mathrm{N}}}(\cdot)$ and $f_{X_{\mathrm{R}}}(\cdot)$ are omitted as they are similar. ■

IV. Coverage Probability and Average Achievable Rate

A. Coverage Probability

The coverage probability is defined as the probability that the SINR at the UE exceeds a predefined threshold. Since the UE can associate with either a L-THz AP, a N-THz AP or an RF AP, the coverage probability can be calculated by using the law of total probability

$$P_{cov} = A_{\mathrm{L}} P_{cov,\mathrm{L}} + A_{\mathrm{N}} P_{cov,\mathrm{N}} + A_{\mathrm{R}} P_{cov,\mathrm{R}}, \tag{24}$$

where A_{L}, A_{N} and A_{R} are the corresponding association probabilities (i.e. the probability of occurrence of the event C_Q, $Q = \{\mathrm{L}, \mathrm{N}, \mathrm{R}\}$) given in (18) and (19) and $P_{cov,\mathrm{L}}$, $P_{cov,\mathrm{N}}$ and $P_{cov,\mathrm{R}}$ are the conditional coverage probabilities given the association status and are derived in the following theorem.

Theorem 1: The conditional coverage probabilities $P_{cov,\mathrm{L}}$, $P_{cov,\mathrm{N}}$ and $P_{cov,\mathrm{R}}$ given that the UE is associated with a LoS THz AP, a NLoS THz AP and RF AP are given by

$$\begin{aligned}P_{cov,\xi} =& \sum_{k=1}^{4} p_{k,0} \mathbb{E}_{x_\xi}\left[\sum_{q=0}^{m_\xi - 1} \frac{(-s_\xi(x_\xi))^q}{q!} \sum_{u=0}^{q} \binom{q}{u} \left(-\frac{\sigma_{\mathrm{T}}^2}{G_k}\right)^{(q-u)}\right.\\ &\left.\times \exp\left(-\frac{s_\xi(x_\xi)\sigma_{\mathrm{T}}^2}{G_k}\right) \frac{\partial^u}{\partial s_\xi^u} \mathcal{L}_{I_\xi}\left(\frac{s_\xi(x_\xi)}{G_k}\right)\right],\end{aligned} \tag{25}$$

$$P_{cov,\mathrm{R}} = \mathbb{E}_{x_{\mathrm{R}}}\left[\mathcal{L}_{I_{\mathrm{R}}}\left(s_{\mathrm{R}}(x_{\mathrm{R}})\right) \exp\left(-s_{\mathrm{R}}\left(x_{\mathrm{R}}\right)\sigma_{\mathrm{R}}^2\right)\right], \tag{26}$$

where $\xi \in \{\mathrm{L}, \mathrm{N}\}$, $s_{\mathrm{R}}(x_{\mathrm{R}}) = \frac{\theta}{P_{\mathrm{R}}\gamma_{\mathrm{R}} x_{\mathrm{R}}^{-\alpha_{\mathrm{R}}}}$, $s_\xi(x_\xi) = \frac{m_{\mathrm{L}}\theta e^{k_a(f_{\mathrm{T}})x_\xi} x_\xi^{\alpha_\xi}}{P_{\mathrm{T}}\gamma_{\mathrm{T}}}$, $\mathcal{L}_{I_\xi}(\cdot)$ and $\mathcal{L}_{I_{\mathrm{R}}}(\cdot)$ represent the Laplace transforms of the interference in the considered association scenarios.

Proof: See Appendix B. Note that the expectation can be solved by deconditionning on the serving distance for each association type using the PDF expressions given in (21) and (21). ■

The obtained coverage expressions, even if failed to lead to closed-form simple expressions, are still a valuable asset for scientific research as they provide a rigorous performance assessment and design paradigm for systems and are in all means less computationally complex and less time consuming than simulations. To be able to derive the expressions of the conditional coverage probabilities, we must find the Laplace transforms of the interference in the three considered association scenarios. Due to the separate spectrum for THz and RF, the UE receives interference signals from the THz APs only when associated with a L-THz or a N-THz AP. Similarly, the UE receives interference from the RF APs only when associated with an RF AP. The interference expressions I_ξ ($\xi \in \{\mathrm{L}, \mathrm{N}\}$) and I_{R} are given in (12) and (10), respectively. The Laplace transforms of I_ξ and I_{R} are given in the following lemmas.

Lemma 3: The Laplace transform of the interference power I_ξ from the THz APs given that the UE is associated with a ξ-THz AP ($\xi \in \{\mathrm{L}, \mathrm{N}\}$) can be given as

$$\begin{aligned}\mathcal{L}_{I_\xi}(s) =& \left[\frac{1}{\int_{x_\xi}^{z_p} f_{\mathrm{Z}}(z)\kappa_\xi(z)\mathrm{d}z + \int_{E_{\xi\bar{\xi}}(x_\xi)}^{z_p} f_{\mathrm{Z}}(z)\kappa_{\bar{\xi}}(z)\mathrm{d}z}\right.\\ &\sum_{k=1}^{4} p_k \left(\int_{x_\xi}^{z_p} f_{\mathrm{Z}}(y)\kappa_\xi(y)\left(1 + \frac{sP_{\mathrm{T}}\gamma_{\mathrm{T}}G_k e^{-k_a(f_{\mathrm{T}})y} y^{-\alpha_\xi}}{m_\xi}\right)^{-m_\xi}\mathrm{d}y\right.\\ &+ \int_{E_{\xi\bar{\xi}}(x_\xi)}^{z_p} \left(1 + \frac{sP_{\mathrm{T}}\gamma_{\mathrm{T}}G_k e^{-k_a(f_{\mathrm{T}})y} y^{-\alpha_{\bar{\xi}}}}{m_{\bar{\xi}}}\right)^{-m_{\bar{\xi}}}\\ &\left.\left.\times f_{\mathrm{Z}}(y)\kappa_{\bar{\xi}}(y)\mathrm{d}y\right)\right]^{\delta_{\mathrm{T}} N_{\mathrm{A}} - 1}.\end{aligned} \tag{27}$$

Proof: See Appendix C. ■

Lemma 4: Given that the UE associates with an RF AP, the Laplace transform of the interference power I_{R} from the remaining RF APs is given by

$$\begin{aligned}\mathcal{L}_{I_{\mathrm{R}}}(s) =& \\ &\left(\frac{1}{\int_{x_{\mathrm{R}}}^{z_p} f_{\mathrm{Z}}(z)\mathrm{d}z} \int_{x_{\mathrm{R}}}^{z_p} \frac{1}{1 + sP_{\mathrm{R}}\gamma_{\mathrm{R}} y^{-\alpha_{\mathrm{R}}}} f_{\mathrm{Z}}(y)\mathrm{d}y\right)^{(1-\delta_{\mathrm{T}})N_{\mathrm{A}} - 1}.\end{aligned} \tag{28}$$

Proof: The interference I_{R} from all interfering RF APs when the UE associates with an RF AP located at x_{R} can be written as $\sum_{i=1}^{(1-\delta_{\mathrm{T}})N_{\mathrm{A}}-1} I_{\mathrm{R},x_i}$, where I_{R,x_i} is the interference from the RF AP located at $\mathbf{x}_i$. Following a similar proof to Lemma 3, the Laplace transform of I_{R}, denoted as $\mathcal{L}_{I_{\mathrm{R}}}(s)$ can be expressed as

$$\mathcal{L}_{I_{\mathrm{R}}}(s) = \left(\mathbb{E}_{I_{\mathrm{R},x_i}}\left[\exp\left(-sI_{\mathrm{R},x_i}\right)\right]\right)^{(1-\delta_{\mathrm{T}})N_{\mathrm{A}}-1}. \tag{29}$$

The expectation term can be calculated as

$$\begin{aligned}&\mathbb{E}_{I_{\mathrm{R},x_i}}\left[\exp\left(-sI_{\mathrm{R},x_i}\right)\right] \overset{(a)}{=} \mathbb{E}_{\chi_{\mathrm{R}},d_{\mathrm{R}}}\left[\exp\left(-sP_{\mathrm{R}}\gamma_{\mathrm{R}} d_{\mathrm{R}}^{-\alpha_{\mathrm{R}}}\chi_{\mathrm{R}}\right)\right]\\ &\overset{(b)}{=} \int_{x_{\mathrm{R}}}^{z_p} \frac{1}{1 + sP_{\mathrm{R}}\gamma_{\mathrm{R}} y_{-\alpha_{\mathrm{R}}}} f_{Y_{\mathrm{R}}}(y, x_{\mathrm{R}})\mathrm{d}y.\end{aligned} \tag{30}$$

where (a) is obtained by omitting the index x_i from the expression of the received power from an RF AP given in Section II-B. (b) is obtained from the moment generating

function (MGF) of the Rayleigh small scale fading gain and by substituting d_{R} with y and averaging over the feasibility range of y. $f_{Y_{\mathrm{R}}}(y, x_{\mathrm{R}})$ is the PDF of the distance from any interfering RF AP located further than x_{R} and is given as $f_{Y_{\mathrm{R}}}(y,x) = \frac{f_Z(y)}{\int_x^{z_p} f_Z(z)\mathrm{d}z}$, where $f_Z(.)$ is given in (13) [47]. By plugging (30) in (29), we can get the final expression in (28). ∎

B. Rate Analysis

In this section, we derive the average achievable rate by using the same analysis conducted for the coverage probability. Thus, the average achievable rate is given in Theorem 2.

Theorem 2: The average achievable DL rate of a UE located at a distance v_0 from the center of a THz/RF coexisting finite indoor network is given by

$$\tau = \tau_{\mathrm{L}} A_{\mathrm{L}} + \tau_{\mathrm{N}} A_{\mathrm{N}} + \tau_{\mathrm{R}} A_{\mathrm{R}}, \tag{31}$$

where A_{L}, A_{N}, and A_{R} are the association probabilities and τ_{L}, τ_{N}, and τ_{R} are the average achievable rates given that the UE associates with a L*-THz AP,* N*-THz AP, or RF AP, and are given by*

$$\begin{aligned}\tau_\xi = {} & \frac{W_{\mathrm{T}}}{\ln 2}\sum_{k=1}^{4} p_{k,0}\int_0^\infty \frac{1}{t+1} \\ & \times \mathbb{E}_{x_\xi}\Bigg[\sum_{q=0}^{m_\xi-1}\frac{(-s_\xi(x_\xi))^q}{q!}\sum_{u=0}^{q}\binom{q}{u}\left(-\frac{\sigma_{\mathrm{T}}^2 t}{G_k\theta}\right)^{(q-u)} \\ & \times \exp\left(-\frac{s_\xi(x_\xi)\sigma_{\mathrm{T}}^2 t}{G_k\theta}\right)\frac{\partial^u}{\partial s_\xi^u}\mathcal{L}_{I_\xi}\left(\frac{s_\xi(x_\xi)t}{G_k\theta}\right)\Bigg]\mathrm{d}t, \end{aligned} \tag{32}$$

$$\begin{aligned}\tau_{\mathrm{R}} = {} & \frac{W_{\mathrm{R}}}{\ln 2}\int_0^\infty \frac{1}{t+1} \\ & \times \mathbb{E}_{x_{\mathrm{R}}}\left[\mathcal{L}_{I_{\mathrm{R}}}\left(\frac{s_{\mathrm{R}}(x_{\mathrm{R}})t}{\theta}\right)\exp\left(-\frac{\sigma_{\mathrm{R}}^2 s_{\mathrm{R}}(x_{\mathrm{R}})t}{\theta}\right)\right]\mathrm{d}t, \end{aligned} \tag{33}$$

where $s_\xi(x_\xi)$ $(\xi \in \{\mathrm{L},\mathrm{N}\})$ and $s_{\mathrm{R}}(x_{\mathrm{R}})$ are given in Theorem 1. W_{T} and W_{R} are the bandwidths used in the THz and the RF communications, respectively. $\mathcal{L}_{I_\xi}(\cdot)$ and $\mathcal{L}_{I_{\mathrm{R}}}(\cdot)$ are the Laplace transforms of the interference for the association scenarios and are provided in (27) and (28).

Proof: Given the Shannon's bound for the instantaneous SINR with a transmission bandwidth W, the average achievable rate for the DL is given by

$$\begin{aligned}\tau = {} & \mathbb{E}\left[W\log_2(1+\mathrm{SINR})\right] \\ \overset{(a)}{=} {} & \int_0^\infty \mathbb{P}\left[W\log_2(1+\mathrm{SINR}) > y\right]\mathrm{d}y \\ \overset{(b)}{=} {} & W_{\mathrm{T}}\int_0^\infty \mathbb{P}\left[\log_2(1+\mathrm{SINR}) > y | C_{\mathrm{L}}\right]\mathrm{d}y A_{\mathrm{L}} \\ & + W_{\mathrm{T}}\int_0^\infty \mathbb{P}\left[\log_2(1+\mathrm{SINR}) > y | C_{\mathrm{N}}\right]\mathrm{d}y A_{\mathrm{N}} \\ & + W_{\mathrm{R}}\int_0^\infty \mathbb{P}\left[\log_2(1+\mathrm{SINR}) > y | C_{\mathrm{R}}\right]\mathrm{d}y A_{\mathrm{R}}, \end{aligned} \tag{34}$$

where W_{T} and W_{R} are the transmission bandwidths for THz and RF. (a) follows from the definition $\mathbb{E}[X] = \int_0^\infty \mathbb{P}[X > y]\,\mathrm{d}y$, and (b) is obtained by referring to the law of total probability and the linearity of integrals. A_{L}, A_{N} and A_{R} are given in (18) and (19). Finally, given that the reference UE is associated with a L-THz AP, the conditional average rate τ_{L} is given by

$$\begin{aligned}\tau_{\mathrm{L}} = {} & W_{\mathrm{T}}\int_0^\infty \mathbb{P}\left[\log_2(1+\mathrm{SINR}_{\mathrm{L}}) > y\right]\mathrm{d}y \\ = {} & \frac{W_{\mathrm{T}}}{\ln 2}\int_0^\infty \mathbb{P}\left[\mathrm{SINR}_{\mathrm{L}} > e^y - 1\right]\mathrm{d}y \\ \overset{(a)}{=} {} & \frac{W_{\mathrm{T}}}{\ln 2}\int_0^\infty \frac{1}{1+t}\mathbb{P}\left[\frac{P_{\mathrm{T}}\gamma_{\mathrm{T}}G_{\mathrm{T},0}e^{-k_a(f_{\mathrm{T}})x_{\mathrm{L}}}x_{\mathrm{L}}^{-\alpha_{\mathrm{L}}}\chi_{\mathrm{L},0}}{I_{\mathrm{L}}+\sigma_{\mathrm{T}}^2} > t\right]\mathrm{d}t \\ \overset{(b)}{=} {} & \frac{W_{\mathrm{T}}}{\ln 2}\int_0^\infty \frac{1}{1+t} \\ & \times \mathbb{E}_{G_{\mathrm{T},0},x_{\mathrm{L}},I_{\mathrm{L}}}\left[\mathbb{P}\left[\chi_{\mathrm{L},0} > \frac{t\left(I_{\mathrm{L}}+\sigma_{\mathrm{T}}^2\right)}{P_{\mathrm{T}}\gamma_{\mathrm{T}}G_{\mathrm{T},0}e^{-k_a(f_{\mathrm{T}})x_{\mathrm{L}}}x_{\mathrm{L}}^{-\alpha_{\mathrm{L}}}}\right]\right]\mathrm{d}t, \end{aligned} \tag{35}$$

where (a) follows from the change of variable $t = e^y - 1$ and from the expression of $\mathrm{SINR}_{\mathrm{L}}$ given in (11) and (b) follows from taking the expectation over x_{L}, I_{L} and $G_{\mathrm{T},0}$. The proof proceeds following the same steps of Theorem 1, therefore we omit it here. Finally, the conditional average achievable rates given that the reference UE is associated with a N-THz AP and with an RF AP can also be derived by following the same proof as that of L-THz AP association. ∎

V. Numerical Results and Discussions

In this section, we study the performance of the proposed RF/THz coexisting network and validate the analytical derivations through Monte-Carlo simulations. We use Mathematica to evaluate the obtained analytical expressions and MATLAB to conduct the simulations. Furthermore, we investigate the effects of different system parameters and provide useful insights. The analysis is focused on a UE located in the center ($\mathbf{v}_0 = (0,0,0)$) of a finite disk of radius $r_d = 80$ m where a fixed number $N_{\mathrm{A}} = 20$ of THz and RF APs are deployed. We adopt the same THz operating frequency ($f_{\mathrm{T}} = 1.05$ THz) and molecular absorption values ($k_a(f_{\mathrm{T}}) = 0.07512$ m^{-1}) as in [28]. These values were calculated for the standard atmosphere with 10% humidity in [11], using a HITRAN-based model [48]. To conduct the simulations, 10^7 network realizations are considered to average over the random APs locations, fading and misalignment. The remaining parameters are as summarized in Table III unless otherwise stated. Note that the shape and dimensions of the user and the blockages represent a realistic indoor scenario and the results provide useful recommendations for optimizing the deployment of THz APs in indoor networks.

A. Numerical Results

Fig. 5 plots the simulation (markers) and analytical (solid lines) results of the THz association probability $A_{\mathrm{T}} = A_{\mathrm{L}} + A_{\mathrm{N}}$ as function of the bias term B_{T} for different values of the beam-steering error on the THz connection. We can see clearly that the analytical results match perfectly with simulations, proving the accuracy of the developed framework and the derived expressions in Lemma 1. The same observation can be noted in Fig. 6 that shows the simulation and analytical results of the coverage probability

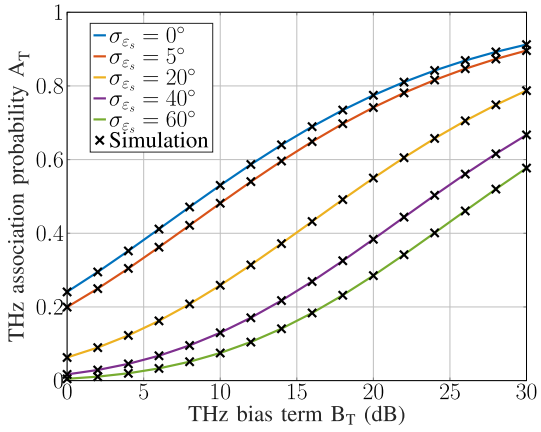

Fig. 5. THz association probability as function of the bias factor B_T for different values of the misalignment error.

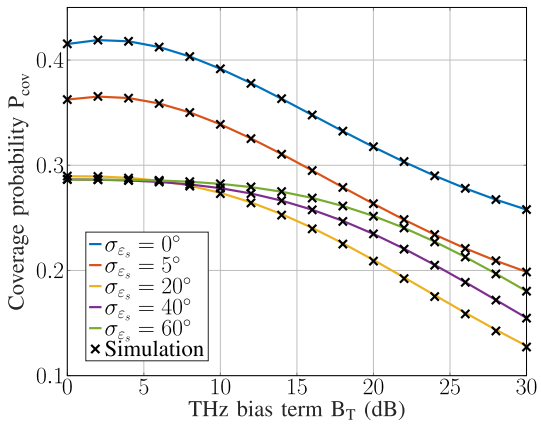

Fig. 6. Coverage probability as function of B_T for different values of the misalignment error.

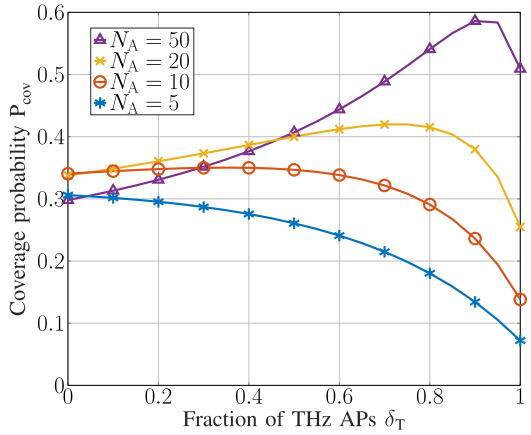

Fig. 7. Coverage probability as function of the fraction of THz APs for different values of the total number of APs.

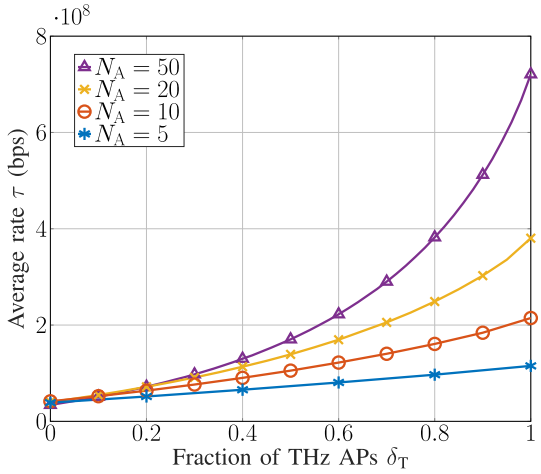

Fig. 8. Average rate as function of the fraction of THz APs for different values of the total number of APs.

as function of B_T for different values of σ_{ε_s}, $s \in \{T, U\}$. Thus, the main analytical findings of this work, which are provided in Theorem 1, are also validated. As expected, the THz association probability increases when the THz bias term increases, allowing us to offload more UEs to THz APs. However, having a high misalignment error on the THz connection limits such offloading as the UE will receive the THz signal through side lobes only, thus with reduced power. An interesting trend can be noticed in Fig. 6; as the variance of the misalignment error increases, the coverage probability decreases. However, when the misalignment error reaches a certain level, the coverage probability starts to increase again. This is not surprising because with high misalignment error levels, the THz-UE link quality deteriorates and the UE is expected to associate more with the existing RF APs which are characterized by higher communication ranges. Thus, the overall coverage probability is improved.

In Fig. 7, we present the coverage probability versus the fraction of THz APs δ_T for different values of the total number of deployed THz and RF APs. The coverage probability starts to increase as δ_T increases. This happens up to a certain level after which adding more THz APs deteriorates the coverage probability. The initial improvement of the coverage probability is achieved because of the high gain directional antennas implemented at THz APs which will reduce the effective interference. However, if the majority of deployed APs are THz APs with limited communication range, there is a higher chance that more UEs will fall into uncovered regions within the deployment area, and we notice a degradation of the coverage probability when $\delta_T \to 1$. For sparse deployments ($N_A \leq 10$), increasing the fraction of THz APs results only in a degradation of the coverage probability due to the limited communication range of THz APs and the limited number of deployed APs which are not sufficient to cover the considered finite area. On the other side, densifying the network ($N_A = 20 \to N_A = 50$) while keeping a low fraction of THz APs reduces the coverage probability which is dominated in this case by the RF tier, thus, increasing the level of RF interference. The impact of interference is mitigated as more THz APs with directional antennas and beam-steering capabilities are introduced.

Fig. 8 demonstrates the impact of the number of deployed APs and the fraction of THz APs δ_T on the average achievable rate in the RF/THz coexisting network. When compared to

TABLE III
SIMULATION PARAMETERS

Parameter	Value	Parameter	Value	Parameter	Value
$(P_{\mathrm{T}}, P_{\mathrm{R}})$	5 dBm	$(f_{\mathrm{T}}, f_{\mathrm{R}})$	1.05 THz, 2.1 GHz	$(\varphi_{\mathrm{T}}, \varphi_{\mathrm{U}})$	$(10^{\circ}, 33^{\circ})$
r_d	80 m	$(W_{\mathrm{T}}, W_{\mathrm{R}})$	0.5 GHz, 40 MHz	$(\sigma_{\varepsilon_{\mathrm{T}}}, \sigma_{\varepsilon_{\mathrm{U}}})$	0°
N_{A}	20	h_{A}	4.5 m	ω_{S}	36°
δ_{T}	0.8	$(m_{\mathrm{L}}, m_{\mathrm{N}})$	(3 , 1)	$(\lambda_{\mathrm{B}}, \lambda_{\mathrm{W}})$	$(0.3, 0.005)$ m^{-2}
(v_0, h_{U})	(0 , 1.4) m	$(\sigma_{\mathrm{T}}^2, \sigma_{\mathrm{R}}^2)$	4×10^{-11}	$(r_{\mathrm{B}}, h_{\mathrm{B}})$	(0.22, 1.7) m
$k_a(f_{\mathrm{T}})$	0.07512 m^{-1}	$(G_{\mathrm{U}}^{(\max)}, G_{\mathrm{U}}^{(\min)})$	(15, -10) dB	$(L_{\mathrm{W}}^{\min}, L_{\mathrm{W}}^{\max})$	(5, 10) m
$(\alpha_{\mathrm{L}}, \alpha_{\mathrm{N}}, \alpha_{\mathrm{R}})$	(2, 4 , 2.7)	$(G_{\mathrm{T}}^{(\max)}, G_{\mathrm{T}}^{(\min)})$	(25, -10) dB	θ	0 dB

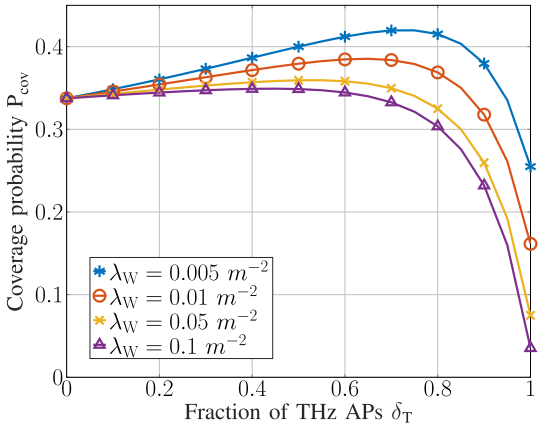

Fig. 9. Coverage probability as function of the fraction of THz APs for different values of the density of wall blockages.

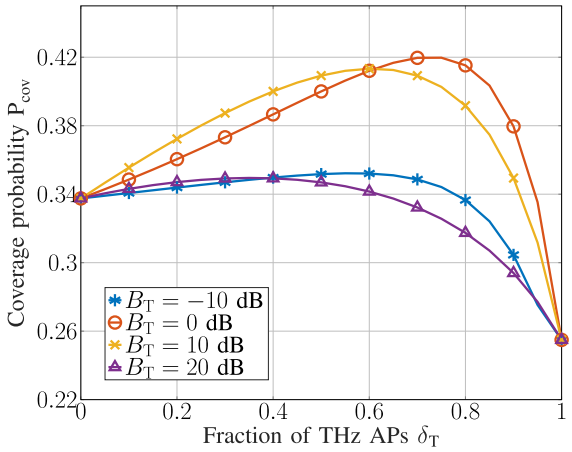

Fig. 10. Coverage probability as function of the fraction of THz APs for different values of the THz bias term.

Fig. 7, a clear trade-off can be noticed; as δ_{T} increases, the average achievable rate significantly increases. Furthermore, densifying the network always improves the rate. This happens regardless of the coverage probability which decreases when THz APs dominate the network. Thus, the fraction of THz APs should be chosen carefully so as to optimize both coverage and rate performance. In fact, due to the low frequency band and limited bandwidth, sub-6 GHz technologies cannot satisfy very high demand for data rates. Such demand entails having small cells that operate at THz frequencies. Now, the coexistence of THz and RF APs together can offer an attractive solution to meet the ever increasing need of ultra-high data rates while overcoming the limited coverage caused by the high absorption losses and high path-loss in THz communications.

In Fig. 9, we present the impact of the walls blockages on the performance of the RF/THz coexisting network. Specifically, Fig. 9 shows the coverage probability as function of the fraction of THz APs for different values of the density of walls blockages λ_{W}. When there are more walls blockers, the likelihood of THz APs being in a NLoS condition becomes higher, which leads to a lower coverage probability. Such effect is better seen at higher fractions of THz deployment since at lower values, the UE tends to associate more with the RF tier, thus the impact of blockages is minimal. As the density of walls increases further, UEs will switch completely to the RF tier and the coverage probability will not change much when more blockers are added.

Fig. 10 shows the coverage probability as function of the fraction of THz APs for different values of the THz bias term. For $B_{\mathrm{T}} = -10$ dB, UEs are encouraged to associate with the RF tier. Such biasing causes a slight increase of the coverage probability as the fraction of THz APs increases and a faster degradation when the network is dominated with THz APs. Furthermore, the performance of the network is worse compared to higher THz biasing as the UE is not benefiting from the advantages that the THz technology provides. The low communication range of THz APs, which is mainly due to high absorption losses, limits the coverage probability that shows an improvement for low biasing values and a degradation as B_{T} increases. For instance, the coverage probability degrades significantly for $B_{\mathrm{T}} = 20$ dB compared to lower biasing values. On the other side, the coverage probability for $B_{\mathrm{T}} = 0$ dB exceeds the case when $B_{\mathrm{T}} = 10$ dB for $\delta_{\mathrm{T}} \leq 0.6$. However, the coverage probability for $B_{\mathrm{T}} = 0$ dB becomes better as δ_{T} further increases. Thus, the optimal bias to THz is larger with lower number of deployed THz APs and UEs are less encouraged to associate with the THz tier as it becomes more dense.

In Fig. 11, we evaluate the impact of the UE location in the finite area on the coverage probability. As the UE moves away from the network center, the coverage probability increases slowly. Such behavior is quite pronounced for low number of deployed THz APs. However, as the UE gets closer to the network edge, the coverage probability drops

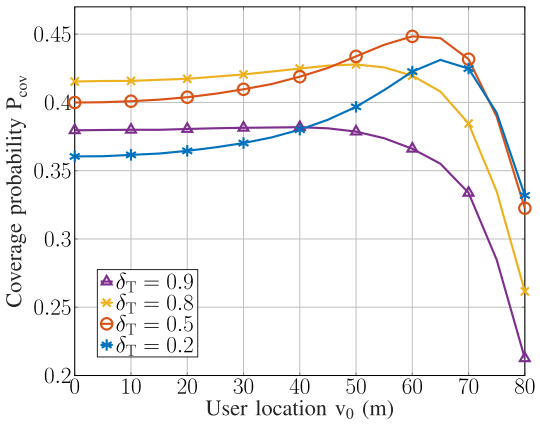

Fig. 11. Coverage probability as function the user's location for different values of the fraction of THz APs.

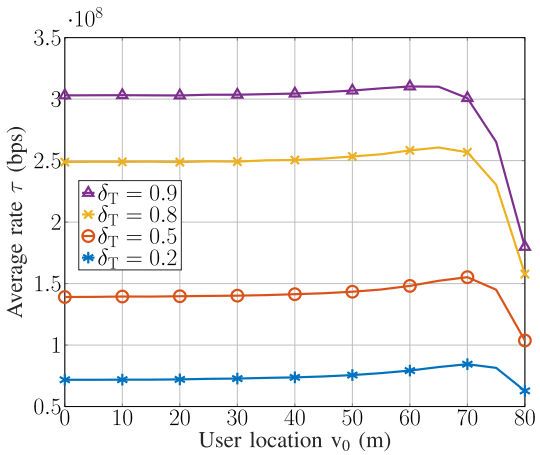

Fig. 12. Average rate as function of the user's location for different values of the fraction of THz APs.

significantly. The initial increase in the coverage probability, when moving away from the center of the network, is caused by the reduction of the RF-dominated interference experienced by the UE due to the border effect of the finite area. Recall that the impact of interference is more severe in RF compared to THz communications because of the added THz-specific losses that limit the communication range, in addition to the highly directional nature of the antennas used for THz. Thus, the improvement of the coverage probability as the UE approaches the network boundary is achieved when RF APs dominate the network. The degradation of the coverage probability at the edge of the network is caused by the reduced likelihood to find a close by AP to serve the UE. Furthermore, central UEs enjoy better coverage performance for high fraction of THz APs δ_T, while edge UEs experience higher coverage probability for low values of δ_T.

The impact of the UE location on the average rate is captured in Fig. 12. The average rate is almost constant when the UE is away from the network boundary and slightly increases when it gets closer because of the reduction of the RF interference. At the edge of the network, the rate degrades due to the boundary effect of the finite BPP. On the other side, increasing the fraction of THz APs always improve the average rate. Fig. 11 and Fig. 12 highlight clearly the importance of taking into consideration the UE location when choosing the best fraction of THz APs to be deployed in a finite area to optimize both the coverage and the achievable rate.

B. Discussions and Key Insights

In this section, we investigate the impacts of different system parameters on the performance of RF/THz coexisting systems in indoor applications to illustrate generic design guidelines and recommendations. Based on the interpretation of Fig. 6 and Fig. 9, we can notice that, the impairments of the THz channel, misalignment errors and existence of blockages limit the benefits of THz communications in terms of increased data rates and bandwidth and force the UEs to stick to the RF tier to get service. The RF/THz coexisting system offers is this case a complete solution in which RF APs complement THz APs to serve the users. Addressing these issues is however mandatory to fully exploit the THz benefits.

An interesting observation found in Fig. 7 is that the use of THz APs instead of RF APs is sparse APs deployments always causes a degradation in the coverage performance as the total number of APs is not sufficient to cover the considered area. On the other side, an optimal fraction of THz APs exists in dense deployments, at which the coverage performance is maximized. The optimal fraction of THz APs is the point at which the user strikes a balance between high beamforming gains and low range for THz communications. A coverage/rate trade-off can be also observed in Fig. 7 and Fig. 8 regarding the fraction of THz APs to be deployed, which demonstrates that improving coverage performance requires moderate THz deployment while high data rates occur when all deployed APs in the coexisting system are THz-based.

Our results in Fig. 10 reveal that biasing the association towards THz APs is not always beneficial. The increased beamforming gains of the antennas arrays implemented at the THz transmitters and receivers slightly improve the coverage probability for low THz biasing. However, the limited communication range of THz propagation leads to uncovered spots in the area of interest and decreases as result the overall coverage. Thus, the THz bias term should be optimized with respect to the number of deployed RF and THz APs in the finite area. The obtained results in Fig. 11 and Fig. 12 reveal the importance of considering the spatial locations of users as a key parameter in the design and optimization of RF/THz coexisting indoor networks. More THz APs are required at the center of the considered area, while denser RF deployment is better to optimize the performance at the edge of the network.

VI. Conclusion

This paper studies a coexisting RF and THz finite network and uses stochastic geometry tools to characterize the coverage probability and average rate. Furthermore, the study incorporates the impact of different system parameters such as the fraction of THz APs, the THz beam-steering error, and

the UE location. Based on the developed framework, we derive tractable expressions for the association probabilities with the THz and the RF tiers, the serving distance distributions, the conditional coverage probabilities, and the average achievable rate. The obtained results reveal that densifying the network with THz APs can improve the rate but negatively affects the coverage probability. Furthermore, a clear trade-off exists between the fraction of THz APs deployed and the bias to the THz tier. Thus, deploying RF and THz APs in a finite area should be carefully planned to achieve ultra-high rates while maintaining sufficient coverage. This work can be extended by studying the uplink of a coexisting RF/THz finite indoor network with power control. Furthermore, the impact of intelligent reflective surfaces in hybrid RF/THz networks can also be investigated.

APPENDIX

A. Proof of Lemma 1

By referring to the association rule, the UE can associate with the AP that offers the strongest average BRSP. The corresponding association probabilities are derived by adopting a similar approach to [49]. Consider an arbitrary AP placed at a distance r from the reference UE, this AP is the serving L-THz AP when three events are simultaneously fulfilled:

- The AP located at a distance r from the UE is a THz AP with LoS connection. Given that δ_{T} is the fraction of THz APs and $\kappa_{\mathrm{L}}(\cdot)$ is the LoS probability, the probability that this event occurs is $\delta_{\mathrm{T}}\kappa_{\mathrm{L}}(r)$.
- For the $(\delta_{\mathrm{T}}N_{\mathrm{A}}-1)$ remaining THz APs, each AP is either a L-THz AP located at a greater distance than r or a N-THz AP located at a greater distance than the exclusion region $E_{\mathrm{LN}}(r)$ given in (15). The probabilities of occurrence of these two cases can be obtained as $\int_r^{z_p} f_{\mathrm{Z}}(z)\kappa_{\mathrm{L}}(z)\mathrm{d}z$ and $\int_{E_{\mathrm{LN}}(r)}^{z_p} f_{\mathrm{Z}}(z)\kappa_{\mathrm{N}}(z)\mathrm{d}z$, respectively, where $f_{\mathrm{Z}}(\cdot)$ is given in (13) and denotes the probability density function (PDF) of the distance from a random AP to the UE and $\kappa_{\mathrm{N}}(\cdot)$ is the NLoS probability. As the two events are mutually exclusive and the remaining $(\delta_{\mathrm{T}}N_{\mathrm{A}}-1)$ THz APs are independent and identically distributed (i.i.d) after conditioning on the location of the reference UE, the probability of achieving this condition is given as $\left(\int_r^{z_p} f_{\mathrm{Z}}(z)\kappa_{\mathrm{L}}(z)\mathrm{d}z+\int_{E_{\mathrm{LN}}(r)}^{z_p} f_{\mathrm{Z}}(z)\kappa_{\mathrm{N}}(z)\mathrm{d}z\right)^{\delta_{\mathrm{T}}N_{\mathrm{A}}-1}$.
- For any of the remaining $(1-\delta_{\mathrm{T}})N_{\mathrm{A}}$ RF APs, it should be located further than the exclusion region $E_{\mathrm{LR}}(r)$ given in (14). Such event can occur with probability $\int_{E_{\mathrm{LR}}(r)}^{z_p} f_{\mathrm{Z}}(z)\mathrm{d}z$. As the $(1-\delta_{\mathrm{T}})N_{\mathrm{A}}$ RF APs are i.i.d after conditioning of the location of the UE, the probability of this condition is given as $\left(\int_{E_{\mathrm{LR}}(r)}^{z_p} f_{\mathrm{Z}}(z)\mathrm{d}z\right)^{(1-\delta_{\mathrm{T}})N_{\mathrm{A}}}$.

As the three conditions above are independent, we can derive the probability that the L-THz AP at distance r is the serving AP as the multiplication of the probabilities of the three events. Finally, there are N_{A} ways of choosing an AP from the BPP set of APs Φ_{A}. As a result, the probability that the UE is associated with a L-THz AP located at distance r is given by:

$$N_{\mathrm{A}}\delta_{\mathrm{T}}\kappa_{\mathrm{L}}(r)\left(\int_r^{z_p} f_{\mathrm{Z}}(z)\kappa_{\mathrm{L}}(z)\mathrm{d}z+\int_{E_{\mathrm{LN}}(r)}^{z_p} f_{\mathrm{Z}}(z)\kappa_{\mathrm{N}}(z)\mathrm{d}z\right)^{\delta_{\mathrm{T}}N_{\mathrm{A}}-1}\left(\int_{E_{\mathrm{LR}}(r)}^{z_p} f_{\mathrm{Z}}(z)\mathrm{d}z\right)^{(1-\delta_{\mathrm{T}})N_{\mathrm{A}}}. \tag{36}$$

The final expression of the association probability with a L-THz AP A_{L} given in (18) can be derived by integrating over $z_l \le r \le z_p$.

B. Proof of Theorem 1

The conditional coverage probability $P_{cov,\mathrm{L}}$ given that the UE associates with a L-THz AP located at x_{L} (i.e. the event C_{L} occurs) is derived as

$$\begin{aligned}
P_{cov,\mathrm{L}} &= \mathbb{P}\left[\mathrm{SINR}\ge\theta|C_{\mathrm{L}}\right]\\
&= \mathbb{P}\left[\mathrm{SINR}_{\mathrm{L}}\ge\theta\right]=\mathrm{P}\left[\frac{P_{\mathrm{T}}\gamma_{\mathrm{T}}G_{\mathrm{T},0}e^{-k_a(f_{\mathrm{T}})x_{\mathrm{L}}}x_{\mathrm{L}}^{-\alpha_{\mathrm{L}}}\chi_{\mathrm{L},0}}{I_{\mathrm{L}}+\sigma_{\mathrm{T}}^2}\ge\theta\right]\\
&\overset{(a)}{=}\mathbb{E}_{G_{\mathrm{T},0},x_{\mathrm{L}},I_{\mathrm{L}}}\left[\mathbb{P}\left[\chi_{\mathrm{L},0}\ge\frac{\theta(I_{\mathrm{L}}+\sigma_{\mathrm{T}}^2)}{P_{\mathrm{T}}\gamma_{\mathrm{T}}G_{\mathrm{T},0}e^{-k_a(f_{\mathrm{T}})x_{\mathrm{L}}}x_{\mathrm{L}}^{-\alpha_{\mathrm{L}}}}\right]\right]\\
&\overset{(b)}{=}\sum_{k=1}^{4}p_{k,0}\mathbb{E}_{x_{\mathrm{L}},I_{\mathrm{L}}}\left[\sum_{q=0}^{m_{\mathrm{L}}-1}\frac{1}{q!}\left(\frac{m_{\mathrm{L}}\theta(I_{\mathrm{L}}+\sigma_{\mathrm{T}}^2)}{P_{\mathrm{T}}\gamma_{\mathrm{T}}G_k e^{-k_a(f_{\mathrm{T}})x_{\mathrm{L}}}x_{\mathrm{L}}^{-\alpha_{\mathrm{L}}}}\right)^q\right.\\
&\left.\times\exp\left(-\frac{m_{\mathrm{L}}\theta(I_{\mathrm{L}}+\sigma_{\mathrm{T}}^2)}{P_{\mathrm{T}}\gamma_{\mathrm{T}}G_k e^{-k_a(f_{\mathrm{T}})x_{\mathrm{L}}}x_{\mathrm{L}}^{-\alpha_{\mathrm{L}}}}\right)\right]\\
&\overset{(c)}{=}\sum_{k=1}^{4}p_{k,0}\mathbb{E}_{x_{\mathrm{L}},I_{\mathrm{L}}}\left[\sum_{q=0}^{m_{\mathrm{L}}-1}\frac{(s_{\mathrm{L}}(x_{\mathrm{L}}))^q}{q!}\left(\frac{I_{\mathrm{L}}+\sigma_{\mathrm{T}}^2}{G_k}\right)^q\right.\\
&\left.\times\exp\left(-\frac{I_{\mathrm{L}}+\sigma_{\mathrm{T}}^2}{G_k}s_{\mathrm{L}}(x_{\mathrm{L}})\right)\right]\\
&\overset{(d)}{=}\sum_{k=1}^{4}p_{k,0}\mathbb{E}_{x_{\mathrm{L}}}\left[\sum_{q=0}^{m_{\mathrm{L}}-1}\frac{(-s_{\mathrm{L}}(x_{\mathrm{L}}))^q}{q!}\left[\frac{\partial^q}{\partial s_{\mathrm{L}}^q}\exp\left(-\frac{\sigma_{\mathrm{T}}^2 s_{\mathrm{L}}(x_{\mathrm{L}})}{G_{\mathrm{k}}}\right)\right.\right.\\
&\left.\left.\times\mathcal{L}_{I_{\mathrm{L}}}\left(\frac{s_{\mathrm{L}}(x_{\mathrm{L}})}{G_k}\right)\right]\right],
\end{aligned}\tag{37}$$

where (a) is obtained by averaging the conditional coverage probability over $\{G_{\mathrm{T},0},x_{\mathrm{L}},I_{\mathrm{L}}\}$ and from exploiting the independence between them. (b) follows from the CCDF of the Nakagami small-scale fading gain $\chi_{\mathrm{L},0}$ given in (6) and from averaging over the discrete random variable $G_{\mathrm{T},0}$ corresponding to the directionality gain of the desired link whose PMF is given in Table II. (c) is obtained from denoting $s_{\mathrm{L}}(x_{\mathrm{L}})=\frac{m_{\mathrm{L}}\theta e^{k_a(f_{\mathrm{T}})x_{\mathrm{L}}}x_{\mathrm{L}}^{\alpha_{\mathrm{L}}}}{P_{\mathrm{T}}\gamma_{\mathrm{T}}}$ and (d) is obtained from the partial derivative expression of the exponential term and from the Laplace transform definition $\mathcal{L}_{I_{\mathrm{L}}}(s)=\mathbb{E}_{I_{\mathrm{L}}}\left[e^{-sI_{\mathrm{L}}}\right]$. The final expression of $P_{cov,\mathrm{L}}$ given in (25) is obtained from applying the expression:

$$\frac{\partial^q}{\partial x^q}f(x)g(x)=\sum_{u=0}^{q}\binom{q}{u}\frac{\partial^u}{\partial x^u}f(x)\frac{\partial^{q-u}}{\partial x^{q-u}}g(x). \tag{38}$$

The conditional coverage probability $P_{cov,\mathrm{N}}$ when the UE is associated with a N-THz AP located at x_{N} (i.e. the event C_{N} occurs) is obtained following the same procedure as $P_{cov,\mathrm{L}}$. Finally, the conditional coverage probability $P_{cov,\mathrm{R}}$ when the

UE associates with an RF AP located at x_{R} (i.e. the event C_{R} occurs) is

$$\begin{aligned} P_{cov,\mathrm{R}} &= \mathbb{P}\left[\mathrm{SINR} \geq \theta | C_{\mathrm{R}}\right] = \mathbb{P}\left[\mathrm{SINR}_{\mathrm{R}} \geq \theta\right] \\ &= \mathbb{P}\left[\frac{P_{\mathrm{R}}\gamma_{\mathrm{R}} x_{\mathrm{R}}^{-\alpha_{\mathrm{R}}}\chi_{\mathrm{R},0}}{I_{\mathrm{R}} + \sigma_{\mathrm{R}}^2} \geq \theta\right] \\ &\overset{(a)}{=} \mathbb{E}_{x_{\mathrm{R}}, I_{\mathrm{R}}}\left[\mathbb{P}\left[\chi_{\mathrm{R},0} \geq \frac{\theta(I_{\mathrm{R}} + \sigma_{\mathrm{R}}^2)}{P_{\mathrm{R}}\gamma_{\mathrm{R}} x_{\mathrm{R}}^{-\alpha_{\mathrm{R}}}}\right]\right] \\ &\overset{(b)}{=} \mathbb{E}_{x_{\mathrm{R}}}\left[\exp\left(-\frac{\theta\sigma_{\mathrm{R}}^2}{P_{\mathrm{R}}\gamma_{\mathrm{R}} x_{\mathrm{R}}^{-\alpha_{\mathrm{R}}}}\right)\right. \\ &\quad \left.\times\, \mathbb{E}_{I_{\mathrm{R}}}\left[\exp\left(-\frac{\theta I_{\mathrm{R}}}{P_{\mathrm{R}}\gamma_{\mathrm{R}} x_{\mathrm{R}}^{-\alpha_{\mathrm{R}}}}\right)\right]\right], \end{aligned} \tag{39}$$

where (a) follows from averaging over the independent random variables $\{x_{\mathrm{R}}, I_{\mathrm{R}}\}$ and (b) from the CCDF of the exponential small scale fading $\chi_{\mathrm{R},0}$. The expression given in (26) is obtained by denoting $s_{\mathrm{R}}(x_{\mathrm{R}}) = \frac{\theta}{P_{\mathrm{R}}\gamma_{\mathrm{R}} x_{\mathrm{R}}^{-\alpha_{\mathrm{R}}}}$ and from the definition of the Laplace transform of I_{R}.

C. Proof of Lemma 3

To derive the Laplace transform of the interference I_{L} from the THz APs in the case when the UE is associated with a L-THz AP placed at a distance x_{L} from the UE, we refer to a similar procedure to [49]. Note here that I_{L} includes the interference from both the L-THz and N-THz APs except the serving AP and is given in (12). I_{L} can also be expressed as $I_{\mathrm{L}} = \sum_{i=1}^{\delta_{\mathrm{T}} N_{\mathrm{A}}-1} I_{\mathrm{L},x_i}$, where I_{L,x_i} is the interference from the THz AP located at $\mathbf{x}_i$. For any of the $(\delta_{\mathrm{T}} N_{\mathrm{A}} - 1)$ interfering THz APs, it can be a L-THz AP located at a greater than x_{L} or a N-THz AP located at a greater distance than $E_{\mathrm{LN}}(x_{\mathrm{L}})$. The probabilities of occurrence of these two events are

$$\frac{\int_{x_{\mathrm{L}}}^{z_p} f_{\mathrm{Z}}(z)\kappa_{\mathrm{L}}(z)\mathrm{d}z}{\int_{x_{\mathrm{L}}}^{z_p} f_{\mathrm{Z}}(z)\kappa_{\mathrm{L}}(z)\mathrm{d}z + \int_{E_{\mathrm{LN}}(x_{\mathrm{L}})}^{z_p} f_{\mathrm{Z}}(z)\kappa_{\mathrm{N}}(z)\mathrm{d}z}$$

and

$$\frac{\int_{E_{\mathrm{LN}}(x_{\mathrm{L}})}^{z_p} f_{\mathrm{Z}}(z)\kappa_{\mathrm{N}}(z)\mathrm{d}z}{\int_{x_{\mathrm{L}}}^{z_p} f_{\mathrm{Z}}(z)\kappa_{\mathrm{L}}(z)\mathrm{d}z + \int_{E_{\mathrm{LN}}(x_{\mathrm{L}})}^{z_p} f_{\mathrm{Z}}(z)\kappa_{\mathrm{N}}(z)\mathrm{d}z},$$

respectively. The Laplace transform $\mathcal{L}_{I_{\mathrm{L}}}(s)$ is given as

$$\begin{aligned} \mathcal{L}_{I_{\mathrm{L}}}(s) &= \mathbb{E}_{I_{\mathrm{L}}}\left[e^{-sI_{\mathrm{L}}}\right] \\ &= \mathbb{E}_{I_{\mathrm{L}}}\left[\exp\left(-s\sum_{i=1}^{\delta_{\mathrm{T}} N_{\mathrm{A}}-1} I_{\mathrm{L},x_i}\right)\right] \\ &\overset{(a)}{=} \prod_{i=1}^{\delta_{\mathrm{T}} N_{\mathrm{A}}-1} \mathbb{E}_{I_{\mathrm{L},x_i}}\left[\exp\left(-sI_{\mathrm{L},x_i}\right)\right] \\ &= \left(\mathbb{E}_{I_{\mathrm{L},x_i}}\left[\exp\left(-sI_{\mathrm{L},x_i}\right)\right]\right)^{\delta_{\mathrm{T}} N_{\mathrm{A}}-1}, \end{aligned} \tag{40}$$

where (a) is induced from the i.i.d distribution of the small scale fading gains and from their independence of the interferers distances and the directionality gains in the interference expression. The expectation term $\mathbb{E}_{I_{\mathrm{L},x_i}}\left[\exp\left(-sI_{\mathrm{L},x_i}\right)\right]$ can be calculated as

$$\begin{aligned} &\mathbb{E}_{I_{\mathrm{L},x_i}}\left[\exp\left(-sI_{\mathrm{L},x_i}\right)\right] \\ &= \frac{\int_{x_{\mathrm{L}}}^{z_p} f_{\mathrm{Z}}(z)\kappa_{\mathrm{L}}(z)\mathrm{d}z}{\int_{x_{\mathrm{L}}}^{z_p} f_{\mathrm{Z}}(z)\kappa_{\mathrm{L}}(z)\mathrm{d}z + \int_{E_{\mathrm{LN}}(x_{\mathrm{L}})}^{z_p} f_{\mathrm{Z}}(z)\kappa_{\mathrm{N}}(z)\mathrm{d}z} \\ &\quad \times \mathbb{E}_{P^r_{\mathrm{L},x_i}}\left[\exp\left(-sP^r_{\mathrm{L},x_i}\right)\right] \\ &\quad + \frac{\int_{E_{\mathrm{LN}}(x_{\mathrm{L}})}^{z_p} f_{\mathrm{Z}}(z)\kappa_{\mathrm{N}}(z)\mathrm{d}z}{\int_{x_{\mathrm{L}}}^{z_p} f_{\mathrm{Z}}(z)\kappa_{\mathrm{L}}(z)\mathrm{d}z + \int_{E_{\mathrm{LN}}(x_{\mathrm{L}})}^{z_p} f_{\mathrm{Z}}(z)\kappa_{\mathrm{N}}(z)\mathrm{d}z} \\ &\quad \times \mathbb{E}_{P^r_{\mathrm{N},x_i}}\left[\exp\left(-sP^r_{\mathrm{N},x_i}\right)\right], \end{aligned} \tag{41}$$

where P^r_{L,x_i} and P^r_{N,x_i} are the received powers from the interfering L-THz AP at $\mathbf{x}_i$ and the N-THz AP at $\mathbf{x}_i$ given in Section II-C. $\mathbb{E}_{P^r_{\mathrm{L},x_i}}\left[\exp\left(-sP^r_{\mathrm{L},x_i}\right)\right]$ can be obtained as

$$\begin{aligned} &\mathbb{E}_{P^r_{\mathrm{L},x_i}}\left[\exp\left(-sP^r_{\mathrm{L},x_i}\right)\right] \\ &\overset{(a)}{=} \mathbb{E}_{G_{\mathrm{T}},\chi_{\mathrm{L}},d_{\mathrm{L}}}\left[\exp\left(-sP_{\mathrm{T}}\gamma_{\mathrm{T}} G_{\mathrm{T}} e^{-k_a(f_{\mathrm{T}})d_{\mathrm{L}}} d_{\mathrm{L}}^{-\alpha_{\mathrm{L}}}\chi_{\mathrm{L}}\right)\right] \\ &\overset{(b)}{=} \sum_{k=1}^{4} p_k \mathbb{E}_{d_{\mathrm{L}}}\left[\left(1 + \frac{sP_{\mathrm{T}}\gamma_{\mathrm{T}} G_k e^{k_a(f_{\mathrm{T}})d_{\mathrm{L}}} d_{\mathrm{L}}^{-\alpha_{\mathrm{L}}}}{m_{\mathrm{L}}}\right)^{-m_{\mathrm{L}}}\right] \\ &\overset{(c)}{=} \sum_{k=1}^{4} p_k \int_{x_{\mathrm{L}}}^{z_p}\left(1 + \frac{sP_{\mathrm{T}}\gamma_{\mathrm{T}} G_k e^{k_a(f_{\mathrm{T}})y} y^{-\alpha_{\mathrm{L}}}}{m_{\mathrm{L}}}\right)^{-m_{\mathrm{L}}} \\ &\quad \times f_{Y_{\mathrm{L}}}(y, x_{\mathrm{L}})\mathrm{d}y, \end{aligned} \tag{42}$$

where (a) is obtained from replacing P_{L,x_i} with its expression and omitting the index x_i. (b) is obtained from averaging over the discrete random variable G_{T} that corresponds to the directionality gain of the interfering link where p_k and G_k are given in Table II and from the moment generating functional (MGF) of the small scale fading gain χ_{L} modeled as a gamma distribution. Finally, (c) follows from substituting d_{L} with y and averaging over y where $f_{Y_{\mathrm{L}}}(y, x_{\mathrm{L}})$ is the distance distribution from an interfering L-THz AP located further that x_{L} and is given in [22, Lemma 4] as $f_{Y_{\mathrm{L}}}(y, x) = \frac{f_{\mathrm{Z}}(y)\kappa_{\mathrm{L}}(y)}{\int_x^{z_p} f_{\mathrm{Z}}(z)\kappa_{\mathrm{L}}(z)\mathrm{d}z}$. Similarly, for a N-THz AP:

$$\begin{aligned} &\mathbb{E}_{P^r_{\mathrm{N},x_i}}\left[\exp\left(-sP^r_{\mathrm{N},x_i}\right)\right] \\ &= \sum_{k=1}^{4} p_k \int_{E_{\mathrm{LN}}(x_{\mathrm{L}})}^{z_p}\left(1 + \frac{sP_{\mathrm{T}}\gamma_{\mathrm{T}} G_k e^{k_a(f_{\mathrm{T}})y} y^{-\alpha_{\mathrm{N}}}}{m_{\mathrm{N}}}\right)^{-m_{\mathrm{N}}} \\ &\quad \times f_{Y_{\mathrm{N}}}(y, E_{\mathrm{LN}}(x_{\mathrm{L}}))\mathrm{d}y, \end{aligned} \tag{43}$$

where $f_{Y_{\mathrm{N}}}(y, E_{\mathrm{LN}}(x_{\mathrm{L}})) = \frac{f_{\mathrm{Z}}(y)\kappa_{\mathrm{N}}(y)}{\int_{E_{\mathrm{LN}}(x_{\mathrm{L}})}^{z_p} f_{\mathrm{Z}}(z)\kappa_{\mathrm{N}}(z)\mathrm{d}z}$ is the distance distribution from a N-THz interfering AP located further than $E_{\mathrm{LN}}(x_{\mathrm{L}})$. By plugging (42), (43) and (41) in (40), we can get the final expression in (27).

REFERENCES

[1] J. G. Andrews et al., "What will 5G be?" *IEEE J. Sel. Areas Commun.*, vol. 32, no. 6, pp. 1065–1082, Jun. 2014.

[2] H. Sarieddeen, N. Saeed, T. Y. Al-Naffouri, and M.-S. Alouini, "Next generation terahertz communications: A rendezvous of sensing, imaging, and localization," *IEEE Commun. Mag.*, vol. 58, no. 5, pp. 69–75, May 2020.

[3] H. Elayan, O. Amin, B. Shihada, R. M. Shubair, and M.-S. Alouini, "Terahertz band: The last piece of RF spectrum puzzle for communication systems," *IEEE Open J. Commun. Soc.*, vol. 1, pp. 1–32, 2020.

[4] N. Rajatheva et al., "Scoring the terabit/s goal: Broadband connectivity in 6G," 2020, *arXiv:2008.07220*.

[5] A. Magbool, H. Sarieddeen, N. Kouzayha, M.-S. Alouini, and T. Y. Al-Naffouri, "Terahertz-band non-orthogonal multiple access: System- and link-level considerations," *IEEE Wireless Commun.*, early access, May 9, 2022, doi: 10.1109/MWC.014.2100654.

[6] Z. Zhang et al., "6G wireless networks: Vision, requirements, architecture, and key technologies," *IEEE Veh. Technol. Mag.*, vol. 14, no. 3, pp. 28–41, Sep. 2019.

[7] C. De Lima et al., "Convergent communication, sensing and localization in 6G systems: An overview of technologies, opportunities and challenges," *IEEE Access*, vol. 9, pp. 26902–26925, 2021.

[8] I. F. Akyildiz, J. M. Jornet, and C. Han, "Terahertz band: Next frontier for wireless communications," *Phys. Commun.*, vol. 12, pp. 16–32, Sep. 2014.

[9] H. Sarieddeen, M.-S. Alouini, and T. Y. Al-Naffouri, "An overview of signal processing techniques for terahertz communications," *Proc. IEEE*, vol. 109, no. 10, pp. 1628–1665, Oct. 2021.

[10] S. Tarboush et al., "TeraMIMO: A channel simulator for wideband ultra-massive MIMO terahertz communications," *IEEE Trans. Veh. Technol.*, vol. 70, no. 12, pp. 12325–12341, Dec. 2021.

[11] J. M. Jornet and I. F. Akyildiz, "Channel modeling and capacity analysis for electromagnetic wireless nanonetworks in the terahertz band," *IEEE Trans. Wireless Commun.*, vol. 10, no. 10, pp. 3211–3221, Oct. 2011.

[12] C. Han, A. O. Bicen, and I. F. Akyildiz, "Multi-wideband waveform design for distance-adaptive wireless communications in the terahertz band," *IEEE Trans. Signal Process.*, vol. 64, no. 4, pp. 910–922, Feb. 2016.

[13] I. F. Akyildiz, C. Han, and S. Nie, "Combating the distance problem in the millimeter wave and terahertz frequency bands," *IEEE Commun. Mag.*, vol. 56, no. 6, pp. 102–108, Jun. 2018.

[14] N. R. Olson, J. G. Andrews, and R. W. Heath, "Coverage and capacity of terahertz cellular networks with joint transmission," *IEEE Trans. Wireless Commun.*, vol. 21, no. 11, pp. 9865–9878, Nov. 2022.

[15] Y. Chen, Y. Li, C. Han, Z. Yu, and G. Wang, "Channel measurement and ray-tracing-statistical hybrid modeling for low-terahertz indoor communications," *IEEE Trans. Wireless Commun.*, vol. 20, no. 12, pp. 8163–8176, Dec. 2021.

[16] A. Faisal, H. Sarieddeen, H. Dahrouj, T. Y. Al-Naffouri, and M.-S. Alouini, "Ultramassive MIMO systems at terahertz bands: Prospects and challenges," *IEEE Veh. Technol. Mag.*, vol. 15, no. 4, pp. 33–42, Dec. 2020.

[17] A. A. Boulogeorgos and A. Alexiou, "Error analysis of mixed THz-RF wireless systems," *IEEE Commun. Lett.*, vol. 24, no. 2, pp. 277–281, Feb. 2020.

[18] H. ElSawy, A. Sultan-Salem, M. S. Alouini, and M. Z. Win, "Modeling and analysis of cellular networks using stochastic geometry: A tutorial," *IEEE Commun. Surveys Tuts.*, vol. 19, no. 1, pp. 167–203, 1st Quart., 2017.

[19] J. Kokkoniemi, J. Lehtomäki, and M. Juntti, "Stochastic geometry analysis for mean interference power and outage probability in THz networks," *IEEE Trans. Wireless Commun.*, vol. 16, no. 5, pp. 3017–3028, Mar. 2017.

[20] V. Petrov, M. Komarov, D. Moltchanov, J. M. Jornet, and Y. Koucheryavy, "Interference and SINR in millimeter wave and terahertz communication systems with blocking and directional antennas," *IEEE Trans. Wireless Commun.*, vol. 16, no. 3, pp. 1791–1808, Mar. 2017.

[21] X.-W. Yao, C.-C. Wang, W.-L. Wang, and C. Han, "Stochastic geometry analysis of interference and coverage in terahertz networks," *Nano Commun. Netw.*, vol. 13, pp. 9–19, Sep. 2017.

[22] C.-C. Wang, X.-W. Yao, C. Han, and W.-L. Wang, "Interference and coverage analysis for terahertz band communication in nanonetworks," in *Proc. IEEE Global Commun. Conf. (GLOBECOM)*, Dec. 2017, pp. 1–6.

[23] D. Moltchanov, P. Kustarev, and Y. Koucheryavy, "Analytical approximations for interference and SIR densities in terahertz systems with atmospheric absorption, directional antennas and blocking," *Phys. Commun.*, vol. 26, pp. 21–30, Feb. 2018.

[24] K. Humadi, I. Trigui, W.-P. Zhu, and W. Ajib, "Coverage analysis of user-centric dense terahertz networks," *IEEE Commun. Lett.*, vol. 25, no. 9, pp. 2864–2868, Sep. 2021.

[25] K. M. S. Huq, J. Rodriguez, and I. E. Otung, "3D network modeling for THz-enabled ultra-fast dense networks: A 6G perspective," *IEEE Commun. Standards Mag.*, vol. 5, no. 2, pp. 84–90, Jun. 2021.

[26] Y. Wu and C. Han, "Interference and coverage analysis for indoor terahertz wireless local area networks," in *Proc. IEEE Globecom Workshops (GC Wkshps)*, Dec. 2019, pp. 1–6.

[27] Y. Wu, J. Kokkoniemi, C. Han, and M. Juntti, "Interference and coverage analysis for terahertz networks with indoor blockage effects and line-of-sight access point association," *IEEE Trans. Wireless Commun.*, vol. 20, no. 3, pp. 1472–1486, Mar. 2021.

[28] A. Shafie, N. Yang, S. Durrani, X. Zhou, C. Han, and M. Juntti, "Coverage analysis for 3D terahertz communication systems," *IEEE J. Sel. Areas Commun.*, vol. 39, no. 6, pp. 1817–1832, Jun. 2021.

[29] A. Shafie, N. Yang, Z. Sun, and S. Durrani, "Coverage analysis for 3D terahertz communication systems with blockage and directional antennas," in *Proc. IEEE Int. Conf. Commun. Workshops (ICC Workshops)*, Jun. 2020, pp. 1–7.

[30] C. Wang and Y. Jin Chun, "Stochastic geometry modeling and analysis for THz-mmWave hybrid IoT networks," 2021, *arXiv:2103.11674*.

[31] J. Sayehvand and H. Tabassum, "Interference and coverage analysis in coexisting RF and dense TeraHertz wireless networks," *IEEE Wireless Commun. Lett.*, vol. 9, no. 10, pp. 1738–1742, Oct. 2020.

[32] M. Shi, X. Gao, A. Meng, and D. Niyato, "Coverage and area spectral efficiency analysis of dense terahertz networks in finite region," *China Commun.*, vol. 18, no. 5, pp. 120–130, May 2021.

[33] A. A. Raja, H. Pervaiz, S. A. Hassan, S. Garg, M. S. Hossain, and M. J. Piran, "Coverage analysis of mmWave and THz-enabled aerial and terrestrial heterogeneous networks," *IEEE Trans. Intell. Transp. Syst.*, vol. 23, no. 11, pp. 1–14, Nov. 2021.

[34] E. Sopin, D. Moltchanov, A. Daraseliya, Y. Koucheryavy, and Y. Gaidamaka, "User association and multi-connectivity strategies in joint terahertz and millimeter wave 6G systems," 2022, *arXiv:2206.03108*.

[35] H. Zheng, J. Zhang, H. Hu, and J. Zhang, "The analysis of indoor wireless communications by a blockage model in ultra-dense networks," in *Proc. IEEE 88th Veh. Technol. Conf. (VTC-Fall)*, Aug. 2018, pp. 1–6.

[36] J. Ye, S. Dang, G. Ma, O. Amin, B. Shihada, and M.-S. Alouini, "On outage performance of terahertz wireless communication systems," *IEEE Trans. Commun.*, vol. 70, no. 1, pp. 649–663, Jan. 2022.

[37] J. Kokkoniemi, J. Lehtomäki, and M. Juntti, "A discussion on molecular absorption noise in the terahertz band," *Nano Commun. Netw.*, vol. 8, pp. 35–45, Jun. 2016.

[38] P. Boronin, D. Moltchanov, and Y. Koucheryavy, "A molecular noise model for THz channels," in *Proc. IEEE Int. Conf. Commun. (ICC)*, Jun. 2015, pp. 1286–1291.

[39] W. Gao, C. Han, and Z. Chen, "Receiver artificial noise aided terahertz secure communications with eavesdropper in close proximity," in *Proc. IEEE Global Commun. Conf. (GLOBECOM)*, Dec. 2020, pp. 1–6.

[40] C. Chaccour, M. N. Soorki, W. Saad, M. Bennis, and P. Popovski, "Can terahertz provide high-rate reliable low-latency communications for wireless VR?" *IEEE Internet Things J.*, vol. 9, no. 12, pp. 9712–9729, Jun. 2022.

[41] M. T. Hossan and H. Tabassum, "Mobility-aware performance in hybrid RF and terahertz wireless networks," *IEEE Trans. Commun.*, vol. 70, no. 2, pp. 1376–1390, Feb. 2022.

[42] V. Petrov, D. Moltchanov, and Y. Koucheryavy, "Interference and SINR in dense terahertz networks," in *Proc. IEEE 82nd Veh. Technol. Conf. (VTC-Fall)*, Sep. 2015, pp. 1–5.

[43] H. Sarieddeen, M.-S. Alouini, and T. Y. Al-Naffouri, "Terahertz-band ultra-massive spatial modulation MIMO," *IEEE J. Sel. Areas Commun.*, vol. 37, no. 9, pp. 2040–2052, Jul. 2019.

[44] T. Bai and R. W. Heath, Jr., "Coverage and rate analysis for millimeter-wave cellular networks," *IEEE Trans. Wireless Commun.*, vol. 14, no. 2, pp. 1100–1114, Feb. 2014.

[45] N. Kouzayha, H. Elsawy, H. Dahrouj, K. Alshaikh, T. Y. Al-Naffouri, and M.-S. Alouini, "Analysis of large scale aerial terrestrial networks with mmWave backhauling," *IEEE Trans. Wireless Commun.*, vol. 20, no. 12, pp. 8362–8380, Dec. 2021.

[46] J. Wildman, P. H. J. Nardelli, M. Latva-Aho, and S. Weber, "On the joint impact of beamwidth and orientation error on throughput in directional wireless Poisson networks," *IEEE Trans. Wireless Commun.*, vol. 13, no. 12, pp. 7072–7085, Dec. 2014.

[47] V. V. Chetlur and H. S. Dhillon, "Downlink coverage analysis for a finite 3-D wireless network of unmanned aerial vehicles," *IEEE Trans. Commun.*, vol. 65, no. 10, pp. 4543–4558, Jul. 2017.
[48] L. S. Rothman et al., "The HITRAN molecular spectroscopic database and HAWKS (HITRAN atmospheric workstation): 1996 edition," *J. Quant. Spectrosc. Radiat. Transf.*, vol. 60, no. 5, pp. 665–710, 1998.
[49] X. Wang, H. Zhang, Y. Tian, and V. C. M. Leung, "Modeling and analysis of aerial base station-assisted cellular networks in finite areas under LoS and NLoS propagation," *IEEE Trans. Wireless Commun.*, vol. 17, no. 10, pp. 6985–7000, Oct. 2018.

Nour Kouzayha (Member, IEEE) received the M.Sc. and M.E. degrees in communications and computer engineering from the Lebanese University, Lebanon, in 2013, and the Ph.D. degree in electrical and computer engineering from the American University of Beirut (AUB), Lebanon. She is currently a Post-Doctoral Fellow with the Information Theory Laboratory, King Abdullah University of Science and Technology (KAUST). From 2018 to 2020, she was a Lecturer at the Computer and Communications Engineering Department, Lebanese International University (LIU). Her research interests are in the area of stochastic geometry for wireless communications, the Internet of Things, UAV-enabled communication systems, and terahertz communications.

Mustafa A. Kishk (Member, IEEE) received the B.Sc. and M.Sc. degrees from Cairo University, Giza, Egypt, in 2013 and 2015, respectively, and the Ph.D. degree from Virginia Tech, Blacksburg, VA, USA, in 2018, all in electrical engineering. He is an Assistant Professor at the Electronic Engineering Department, Maynooth University, Ireland. Before that, he was a Post-Doctoral Research Fellow with the Communication Theory Laboratory, King Abdullah University of Science and Technology, Saudi Arabia. His current research interests include stochastic geometry, UAV-enabled communication systems, and satellite-enabled communications. He was a recipient of the IEEE ComSoc Outstanding Young Researcher Award for Europe, Middle East, and Africa Region, in 2022. He was recognized as an Exemplary Reviewer by the IEEE COMMUNICATIONS LETTERS in 2020. He currently serves as an Associate Editor for IEEE WIRELESS COMMUNICATION LETTERS.

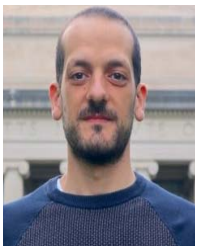

Hadi Sarieddeen (Member, IEEE) received the B.E. degree (summa cum laude) in computer and communications engineering from Notre Dame University–Louaize (NDU) in 2013 and the Ph.D. degree in electrical and computer engineering from the American University of Beirut (AUB) in 2018. He is a Post-Doctoral Associate with the Research Laboratory of Electronics, Massachusetts Institute of Technology (MIT), working in the Network Coding and Reliable Communications Group of Prof. Muriel Médard. Before joining MIT, he was a Post-Doctoral Research Fellow at the King Abdullah University of Science and Technology (KAUST), where he worked with Prof. Mohamed-Slim Alouini and Prof. Tareq Al-Naffouri. His research interests include communication theory, coding theory, and signal processing for wireless communications, with an emphasis on signal processing for terahertz-band communications.

Mohamed-Slim Alouini (Fellow, IEEE) was born in Tunis, Tunisia. He received the Ph.D. degree in electrical engineering from the California Institute of Technology (Caltech), Pasadena, CA, USA, in 1998. He served as a Faculty Member at the University of Minnesota, Minneapolis, MN, USA; and the Texas A&M University, Qatar, Education City, Doha, Qatar, before joining the King Abdullah University of Science and Technology (KAUST), Thuwal, Makkah, Saudi Arabia, as a Professor of electrical engineering, in 2009. His current research interests include modeling, design, and performance analysis of wireless communication systems.

Tareq Y. Al-Naffouri (Senior Member, IEEE) received the B.S. degree (Hons.) in mathematics and electrical engineering from the King Fahd University of Petroleum and Minerals, Dhahran, Saudi Arabia, the M.S. degree in electrical engineering from the Georgia Institute of Technology, and the Ph.D. degree in electrical engineering from Stanford University, in 2004. He was a Visiting Scholar at the California Institute of Technology, Pasadena, CA, USA, in 2005 and Summer 2006. He was a Fulbright Scholar at the University of Southern California in 2008. He is currently a Professor at the Electrical and Computer Engineering Program, King Abdullah University of Science and Technology (KAUST). He has over 300 publications in journal and conference proceedings and 20 issued/pending patents. His research interests lie in the areas of sparse, adaptive, and statistical signal processing and their applications to wireless communications and localization, machine learning, and network information theory. He was a recipient of the IEEE Education Society Chapter Achievement Award in 2008, the Al-Marai Award for Innovative Research in Communication in 2009, and the Abdul Hameed Shoman Arab Researchers Award in 2022. He was an Associate Editor of IEEE TRANSACTIONS ON SIGNAL PROCESSING, from 2013 to 2018.